Cerebral Cortex, August 2018;28: 2817–2833

doi: 10.1093/cercor/bhx161
Advance Access Publication Date: 5 July 2017
Original Article

ORIGINAL ARTICLE

A Layer-specific Corticofugal Input to the Mouse Superior Colliculus

Hector Zurita, Crystal Rock, Jessica Perkins and Alfonso junior Apicella

Department of Biology, Neuroscience Institute, University of Texas at San Antonio, San Antonio, TX 78249, USA

Address correspondence to Dr. Alfonso junior Apicella, Biosciences Building 1.03.26, One UTSA Circle, San Antonio, TX 78249, USA.
Email: alfonso.apicella@utsa.edu

H. Zurita and C. Rock contributed equally to this work

Abstract

In the auditory cortex (AC), corticofugal projections arise from each level of the auditory system and are considered to provide feedback "loops" important to modulate the flow of ascending information. It is well established that the cortex can influence the response of neurons in the superior colliculus (SC) via descending corticofugal projections. However, little is known about the relative contribution of different pyramidal neurons to these projections in the SC. We addressed this question by taking advantage of anterograde and retrograde neuronal tracing to directly examine the laminar distribution, long-range projections, and electrophysiological properties of pyramidal neurons projecting from the AC to the SC of the mouse brain. Here we show that layer 5 cortico-superior-collicular pyramidal neurons act as bandpass filters, resonating with a broad peak at ~3 Hz, whereas layer 6 neurons act as low-pass filters. The dissimilar subthreshold properties of layer 5 and layer 6 cortico-superior-collicular pyramidal neurons can be described by differences in the hyperpolarization-activated cyclic nucleotide-gated cation h-current (I_h). I_h also reduced the summation of short trains of artificial excitatory postsynaptic potentials injected at the soma of layer 5, but not layer 6, cortico-superior-collicular pyramidal neurons, indicating a differential dampening effect of I_h on these neurons.

Key words: auditory cortex, drivers and modulators, hyperpolarization-activated cyclic nucleotide-gated cation h-current (I_h), layer 5 and layer 6, superior colliculus

Introduction

The superior colliculus (SC) is located in the midbrain and is divided into dorsal, intermediate, and deep layers (for review see Stein 1998; and King 2004). The intermediate and the deep layers of the SC process sensory information from different modalities. The integration of this multisensory information in the SC allows an animal to direct behavior responses toward specific locations in space (Sprague and Meikle 1965). Studies in rodents using unilateral pharmacological block of $GABA_A$ receptors, glutamate infusion, electrical stimulation, or optogenetic manipulations in the intermediate and deep layers of the SC have led to the conclusion that the behavior response initiated by the these layers of the SC can be divided in two categories: 1) orienting behavior and 2) avoidance/defense behavior (Redgrave et al. 1981; McHaffie and Stein 1982; Sahibzada et al. 1986; Liang et al. 2015; Zingg et al. 2017).

Manipulations of the SC in other species have shown similar outcomes to what has been reported in rodents. In cats, lesions or deactivation of the SC disrupts orienting behavior (Lomber et al. 2001). In primates, electrical or pharmacological stimulation of the SC induces the animal to orient its head and eyes to the contralateral side of the stimulation (Wurtz and Albano 1980; Hikosaka and Wurtz 1985; Cowie and Robinson 1994). More recently, DesJardin et al. (2013) demonstrated for the first time that an infusion of a $GABA_A$ receptor antagonist in the intermediate and deep layers of the SC leads to defensive-like

behaviors in monkeys. As these results are similar to the observed behaviors in rodents, it is likely that the role of the SC is conserved across species.

The SC receives ascending auditory information from the inferior colliculus (King et al. 1998; Nodal et al. 2005). However, it is also established that the auditory cortex (AC) can directly modulate the response of the SC neurons via descending corticofugal projections (Diamond et al. 1969; Wallace et al. 1993); for review see (Malmierca and Ryugo 2011; Bajo and King 2012; Stebbings et al. 2014). Recently Bajo et al. (2010), in the ferret, and Chabot et al. (2013), in the cat, demonstrated that large pyramidal neurons located primarily in layer 5 of the AC project to the SC. In this study, we investigated the projection from the AC to the SC in mice using a combination of retrograde and anterograde tracing, electrophysiological recordings, and anatomical approaches.

The present study focused on three main goals: 1) determine the laminar distribution of cortico-superior-collicular pyramidal neurons in the AC and their axonal projections in the SC; 2) describe the anatomical and electrophysiological properties of these pyramidal neurons; 3) determine the impact that the hyperpolarization-activated cyclic nucleotide-gated cation h-current (I_h) has on the resonance frequency and synaptic summation. Our approach consisted of anatomical tracing and electrophysiological methods to investigate these questions. Using these manipulations, we found a direct projection from layer 5 and layer 6 pyramidal neurons in the dorsal, primary, and ventral AC to the SC. Our data show these neurons have a different morphology, with the layer 5 pyramidal neurons having an extensive dendritic arborization in layer 1, a feature typical of thick-tufted pyramidal neurons, whereas layer 6 pyramidal neurons lacked this feature. Higher expression of I_h current was characteristic of the layer 5 cortico-superior-collicular pyramidal neurons. The I_h current also reduced both the summation of short trains of artificial excitatory postsynaptic potentials injected at the soma of layer 5 but not layer 6 cortico-superior-collicular pyramidal neurons, and excitatory inputs evoked by electrical stimulation of the AC. Overall, we describe two layer-specific sub-classes of projection neurons to the SC that may serve separate functions in cortico-superior-collicular circuits and that may be engaged differently during defensive–like and/or orienting behavior.

Materials and Methods

Animal procedures were approved by the Institutional Animal Care and Use Program at the University of Texas at San Antonio and followed animal welfare guidelines from the National Institutes of Health.

Mouse Lines

In this study wild-type C57BL/6 (Charles River) and Sim1 KJ18-Cre mice on a CD-1 background (Charles River) were used.

Stereotaxic Injections

Anterograde Labeling

To visualize axons from cortico-superior-collicular pyramidal neurons in the SC, adult C57BL/6 mice (4–6 weeks old) were used for injections of an adeno-associated virus delivering GFP (AAV.GFP; AAV2/1.CamKIIa.4.eGFP.WPRE.rBG, University of Pennsylvania Vector Core). The virus was mixed in a 5:1 ratio with red RetroBeads (Lumafluor) in order to easily identify the injection site. The mice were anesthetized with isoflurane (1–2.5% maintenance) for surgery, which was performed on a stereotaxic frame (Kopf). Between 40–50 nl of the virus was pressure injected (Nanoject II, Drummond Scientific) through a borosilicate glass injection pipette into the AC (2.45 mm posterior to bregma, 4.35 mm lateral to midline, at a depth of 1.0–0.8 mm ventral to the pia). The virus was delivered over a time span of 5–10 min with the glass pipette remaining in place for an additional 5–10 min before being withdrawn.

Three weeks following these injections, these mice were deeply anesthetized with 5% isoflurane and transcardially perfused with phosphate buffered saline (PBS), followed by 10% neutral buffered formalin (Sigma-Aldrich). The brain was carefully removed and fixed for several hours at room temperature. The fixed brain was then sectioned into 200 μm thick slices on a vibrating microtome. After washing in PBS, the slices were mounted on microscope slides with Fluoromount-G mounting medium (Southern Biotech). Confocal images were taken with a Zeiss LSM-710 confocal microscope. Images were rotated, cropped, and the brightness/contrast was adjusted in ImageJ (National Institutes of Health).

To visualize axons from layer 5 cortico-superior-collicular pyramidal neurons in the SC, adult Sim1 KJ18-Cre mice (17–18 weeks old) were injected with a combination of AAV.GFP and AAV.tdTomato.Flex (AAV2/1.CAG.Flex.tdTomato.WPRE.bGH, UNC Vector Core). In these mice, Cre recombinase is expressed in layer 5 projecting-type (PT-type) pyramidal neurons. These injections resulted in non-specific transfection of pyramidal neurons with GFP and targeted transfection of layer 5 PT-type pyramidal neurons with tdTomato. A small amount of red RetroBeads was added to the injection solution in order to easily identify the injection site (images of the injection site containing a large proportion of red RetroBeads were omitted from later analysis due to the overlap between RetroBead and tdTomato fluorescence). The viruses were injected in the AC as described previously.

About 13–17 days following injections, these mice were deeply anesthetized with 5% isoflurane and transcardially perfused with PBS, followed by 10% neutral buffered formalin. The brain was carefully removed and fixed for several hours at room temperature. The fixed brain was then sectioned into 100 μm thick slices on a vibratome. After washing in PBS, the slices were mounted on microscope slides with Fluoromount-G mounting medium containing DAPI (Southern Biotech).

Retrograde Labeling

To identify cortico-superior-collicular pyramidal neurons in the AC, adult C57BL/6 mice (4–6 weeks old) were used for injections of a retrograde tracer into the SC. The same basic surgical procedures were followed as previously described, with approximately 20 nl of a retrograde tracer (RetroBeads, Lumafluor) being injected into the SC (4.05 mm posterior to bregma, 0.835 mm lateral to midline, at a depth of 1.8 mm ventral to bregma). The tracer was delivered over a time span of 3–5 min with the glass pipette remaining in place for an additional 5–10 min before being withdrawn.

In Vitro Slice Preparation and Recordings

About 2–7 days after intracranial injection of a retrograde tracer into the SC, these mice were anesthetized with isoflurane and decapitated. The brains of the animals were dissected and sectioned in a chilled cutting solution (in mM: 110 Choline Chloride, 25 $NaHCO_3$, 2.5 KCl, 1.25 NaH_2PO_4, 0.5 $CaCl_2$, 7 $MgSO_4$, 25 D-glucose, 11.6 Sodium Ascorbate, 3.1 Sodium Pyruvate). Coronal slices containing the primary AC (300 μm, bregma −2.2 to −3.1)

were made using a vibratome (Leica VT1200S, Leica Biosystems). Slices were incubated in oxygenated artificial cerebral spinal fluid (ACSF solution in mM: 127 NaCl, 2.5 KCl, 26 $NaHCO_3$, 2 $CaCl_2$, 1 $MgCl_2$, 1.25 NaH_2PO_4, 25 D-glucose) in a submerged chamber at 35–37°C for 30 min and then at room temperature (21–25°C) until used for recordings.

Fluorescent-bead-labeled cortico-superior-collicular neurons were located in the AC ipsilateral to the injection site in the SC. The AC was identified by the presence of fluorescent tracers. We also used 2 landmarks similar to the ones used in a previous study (Oviedo et al. 2010; Rock and Apicella 2015; Rock et al. 2016). Briefly, we centered the *x*-axis on the boundary between the dorsal and ventral division of the lateral geniculate body, then a perpendicular line, *y*-axis, was drawn using custom software to align the AC from mouse to mouse.

Whole cell recordings were performed at 31–33°C in ASCF solution using pipettes with 3–4 MΩ resistance. Intrinsic properties were recorded using a K-based intracellular solution at 31–33°C (in mM: 20 KCl, 120 potassium gluconate, 10 HEPES, 0.2 EGTA, 4 ATP, 0.3 GTP, 10 mM phosphocreatine, and either 0 or 0.3–0.5% biocytin). Pharmacological blockers used were CPP (5 µM, Tocris), NBQX (10 µM, Abcam), gabazine (1 µM, Abcam), and ZD7288 (20 µM, Tocris). The software program Ephus (Suter et al. 2010) (www.ephus.org) was used for hardware control and data acquisition. Signals were filtered at 4 kHz and sampled at 10 kHz. Pipette capacitance was compensated for and the series resistance during recordings was lower than 20 MΩ. The resting membrane potential (V_m) was calculated in current-clamp mode ($I = 0$) immediately after breaking in. Series (R_s) and input resistance (R_{in}) were calculated in voltage-clamp mode ($V_{hold} = -70$ mV) by giving a −5 mV step, which resulted in transient current responses. R_s was determined by dividing the −5 mV voltage step by the peak current value generated immediately after the step in the command potential. The difference between baseline and steady-state hyperpolarized current (ΔI) was used to calculate R_{in} using the following formula: $R_{in} = -5\text{ mV}/\Delta I - R_s$. Subthreshold and suprathreshold membrane responses in current-clamp were elicited by injecting −100 to +500 pA in 50 pA increments while holding the baseline membrane potential at −70 mV with an injection of the appropriate amount of current. The first resulting action potential (AP) at rheobase was analyzed for AP width. AP half-width was calculated as the half-width at the half-maximum amplitude of the AP. The adaptation ratio was measured at the current step that gave the closest APs firing rate to 20 Hz. Adaptation ratio was calculated by dividing the instantaneous frequency between the 10th and 11th AP by the instantaneous frequency between the 6th and 5th AP (f_{10}/f_5) to prevent the initial burst of APs from influencing our measurement (Fig. 5*e*). Membrane potential sag was measured using a current injection to hyperpolarize the neuron from −70 mV to −90 mV. Membrane potential sag was calculated using the formula: $\text{Sag} = 100X(V_{peak} - V_{steady\text{-}state})/V_{peak}$. Impedance amplitude profiles (ZAPs) were measured in current-clamp mode by applying a subthreshold chirp stimulus (frequency-swept sinusoids ranging linearly between 0–20 Hz over a period of time of 20 s) via the patch pipette while holding the baseline membrane potential at −70 mV with an injection of the appropriate amount of current.

Histology

Cortico-superior-collicular pyramidal neurons were patched with pipettes containing 0.3–0.5% biocytin in the internal solution. Filled neurons were held for 20–40 min and immediately fixed in 10% neutral buffered formalin for 12–48 h. The slices were then washed extensively with PBS and placed in a streptavidin (Alexa Fluor 488 conjugate, Life Technologies) solution (1 mL 0.3% Triton X-100 in PBS, 4 µL streptavidin). After a 2 h room-temperature incubation period, the slices were washed in PBS and mounted with Fluoromount-G mounting medium on a glass slide. Images were taken with a Zeiss LSM-710 confocal microscope at 10–40X magnification.

Morphological Quantification

Individual high magnification images of cortico-superior-collicular pyramidal neurons were stitched together, when necessary, using XuvStitch software (Emmenlauer et al. 2009). Images were rotated, cropped, and the brightness/contrast was adjusted in ImageJ. The dendrites of these neurons were morphologically reconstructed in 3 dimensions using the Simple Neurite Tracer plugin for ImageJ. Cell morphological measurements, including calculation of soma area, dendritic length, number of branches, and Sholl analysis (Sholl 1953), were performed using the Simple Neurite Tracer plugin (Longair et al. 2011; Ferreira et al. 2014) and region of interest measurement tool in ImageJ.

Quantification of Areal Distribution in the AC

Two to four days after intracranial injection of a retrograde tracer into the SC, these mice were deeply anesthetized with 5% isoflurane, perfused, and the brain was fixed using the same procedures as previously described. The fixed brain was then sectioned into 100 µm thick slices on a vibrating microtome. After washing in PBS, the slices were mounted on microscope slides, and images were taken with an Olympus SZX7 microscope. Images of 100 µm thick slices expressing the retrograde label were rotated, cropped, and the brightness/contrast was adjusted in ImageJ. Using Adobe Illustrator, epifluorescence images were overlaid onto images from the Allen Mouse Brain Reference Atlas for coronal slices (Allen Institute for Brain Science) and aligned using anatomical landmarks such as the rhinal fissure and subcortical structures. Dorsal, primary, and ventral areas of the AC were identified using the overlaid reference images.

Quantification of Layer 5 Cortico-Superior-Collicular Pyramidal Neurons in the AC

Images of the AC injection site were collected to analyze the distribution of pyramidal neurons specifically transfected by AAV.tdTomato.Flex in Sim1 KJ18-Cre mice in comparison to non-specific transfection by AAV.GFP. 300 µm wide sections of the AC were analyzed. The distance from the pia to the white matter was normalized to 1000 µm, and the fluorescence was quantified in 100 µm bins using ImageJ. The fluorescence measurement for GFP and tdTomato in each slice was scaled from 0 to 1. The normalized values were then averaged for 12 slices containing the AC from 4 mice.

Quantification of Layer 5 Cortico-Superior-Collicular Axons in the SC

Images of the ipsilateral SC were collected to analyze the distribution of axonal projections specifically transfected by AAV.tdTomato.Flex in Sim1 KJ18-Cre mice in comparison to non-specific transfection by AAV.GFP. Tile scan images to cover the entire SC in a coronal brain slice were acquired at 10X magnification and 12-bit depth with ZEN software (Zeiss) using a Zeiss LSM-710 confocal microscope. Approximate boundaries for the

superficial, intermediate, and deep layers of the SC were drawn as regions of interest in ImageJ based on the Allen Mouse Brain Reference Atlas for coronal slices (example shown in Fig. 3*e*). Background areas of each layer not containing visible axons were also defined as regions of interest. Using the histogram function of ImageJ, the gray values of the pixels in each layer were quantified. The mean and standard deviation of the gray values of the background regions were also quantified. Fluorescent signals in the layers were defined as those pixels with a gray value greater than the mean plus 3 times the standard deviation of the background region of interest for each layer. The number of pixels was then divided by the area which was analyzed in order to obtain the pixels/μm^2 measure reported in Fig. 3*f*. This figure shows the average pixels/μm^2 quantified from 9 slices containing the SC in 3 mice.

Data Analysis

Error bars in all figures represent s.e.m. Data and statistical analysis was performed offline using MATLAB routines (MathWorks). Group data represent the mean ± s.e.m. Group comparisons were made using a Student's *t*-test if the data were normally distributed (assessed with Lilliefors' test) or the rank-sum for non-normally distributed data, with significance defined as $P < 0.05$.

Results

Laminar Distribution of Cortico-Superior-Collicular Pyramidal Neurons in the Mouse

In initial experiments we used an anterograde viral tracing approach in order to determine which region/s of the SC are innervated by the AC (Fig. 1*a*). Figure 1*b* shows an example of an injection of the AAV.GFP construct together with retrograde tracers in the AC. The injection site was centered in the primary AC and extended to the dorsal and ventral AC as well. GFP-labeled terminals were located mostly ipsilateral to the injection site in both the intermediate and deep layers of the SC (Fig. 1*c*).

Next, to visualize long-range projections originating in the AC and terminating in the SC, we injected retrograde tracers (Fig. 1*d*), such as red RetroBeads, into the SC. Figure 1*e* shows an example of an injection site in the SC. The injection site was centered primarily in the intermediate and deep layers of the SC. From the center of the injection, the spread of the tracer was ~300 μm in the anteroposterior plane. For all of our injections ($n = 15$), there was no evidence of tracer deposit or spillover in the inferior colliculus or the periaqueductal gray. These are two brain areas bordering the SC, and are known to receive corticofugal projections from the AC (Bajo et al. 2007; Schofield 2009; Slater et al. 2013). Using this method, we found that cortico-superior-collicular neurons were located in layers 5 and 6 of the AC in the hemisphere ipsilateral to the injection site (Fig. 1*f*). Moreover, retrogradely labeled cortico-superior-collicular neurons were identified throughout the entire AC, including the dorsal, primary, and ventral areas (Fig. 2). The distribution of the retrogradely labeled neurons is indicated in Fig. 2 by overlapping coronal epifluorescence images with reference images from the online mouse atlas provided by the Allen Institute for Brain Science (http://mouse.brain-map.org/static/atlas; coronal atlas). These data show that the entire AC, via layers 5 and 6 cortico-superior-collicular neurons, sends a direct projection to the intermediate and deep layers of the SC.

Distribution of Auditory Corticofugal Projections to the SC

The finding that both layer 5 and layer 6 cortico-superior-collicular pyramidal neurons of the AC project to the SC suggested the possibility that these neurons may innervate the same or different layers of the SC. To visualize these projections in the SC, we conditionally expressed tdTomato in layer 5 projecting-type pyramidal neurons (such as cortico-superior-collicular pyramidal neurons) while simultaneously non-specifically labeling all pyramidal neurons in the AC with GFP by injecting a combination of AAV.GFP and AAV.tdTomato.Flex into the right AC of Sim1 KJ18-Cre transgenic mice (Fig. 3*a*). Between the two viruses we found a similar area of transfection, quantified as the distance from the injection site to the most posterior slice showing either GFP- or tdTomato-expressing soma (GFP: 633 ± 33 μm; tdTomato: 700 ± 58 μm; data not shown). GFP was colocalized with layer 5 projecting-type/tdTomato-expressing pyramidal neurons in the AC (Fig. 3*b*,*c*). This method allowed us to visualize the contribution of both layers 5 and 6 (GFP-expressing axons) and layer 5 alone (tdTomato-expressing axons) long-range projections originating in the cortex and terminating in the SC (Fig. 3*d*,*e*). However, this method does not exclude the possibility that cortico-superior-collicular pyramidal neurons labeled in the Sim1 KJ18-cre mouse line are only a subset layer 5 pyramidal neurons that project to the SC. We further investigated the SC target layers for these axonal projections by dividing the SC into 3 main layers (superficial, intermediate, and deep) and examining the relative fluorescence levels in each. The boundaries for these layers were approximated based on bright-field image landmarks and comparison to the Allen Institute for Brain Science coronal mouse atlas. On the average, both GFP and tdTomato expression was highest in intermediate layers of the SC (Fig. 3*d*–*f*). It is important to note that this approach does not exclude the possibility that layer 6 cortico-superior-collicular pyramidal neurons may target isolated layers in the SC. These results demonstrate that layer 5 cortico-superior-collicular pyramidal neurons as well as non-specifically labeled pyramidal neurons, including layer 6 cortico-superior-collicular pyramidal neurons, in the AC innervate both the intermediate and the deep layers of the SC.

Morphological Properties of Layers 5 and 6 Cortico-Superior-Collicular Pyramidal Neurons in the Mouse AC

Here we test the hypothesis that cortico-superior-collicular pyramidal neurons have different morphological properties according to their layer of origin (Fig. 4*a*). We quantitatively analyzed the morphology of biocytin-filled layer 5 ($n = 10$) and layer 6 ($n = 11$) cortico-superior-collicular pyramidal neurons. Layer 5 cortico-superior-collicular pyramidal neurons had an extensive dendritic arborization in layer 1, a feature typical of thick-tufted pyramidal neurons in other cortical areas, whereas layer 6 cortico-superior-collicular pyramidal neurons lacked this feature (Fig. 4*b*,*g*).

\We empirically determined the location of biocytin-filled layer 5 and layer 6 cortico-superior-collicular pyramidal neurons for each slice. The soma location was measured as the normalized distance between the pia and the white matter. The soma locations of layer 5 and layer 6 cortico-superior-collicular pyramidal neurons were significantly different from each other (layer 5: 0.53 ± 0.01 mm, $n = 10$; layer

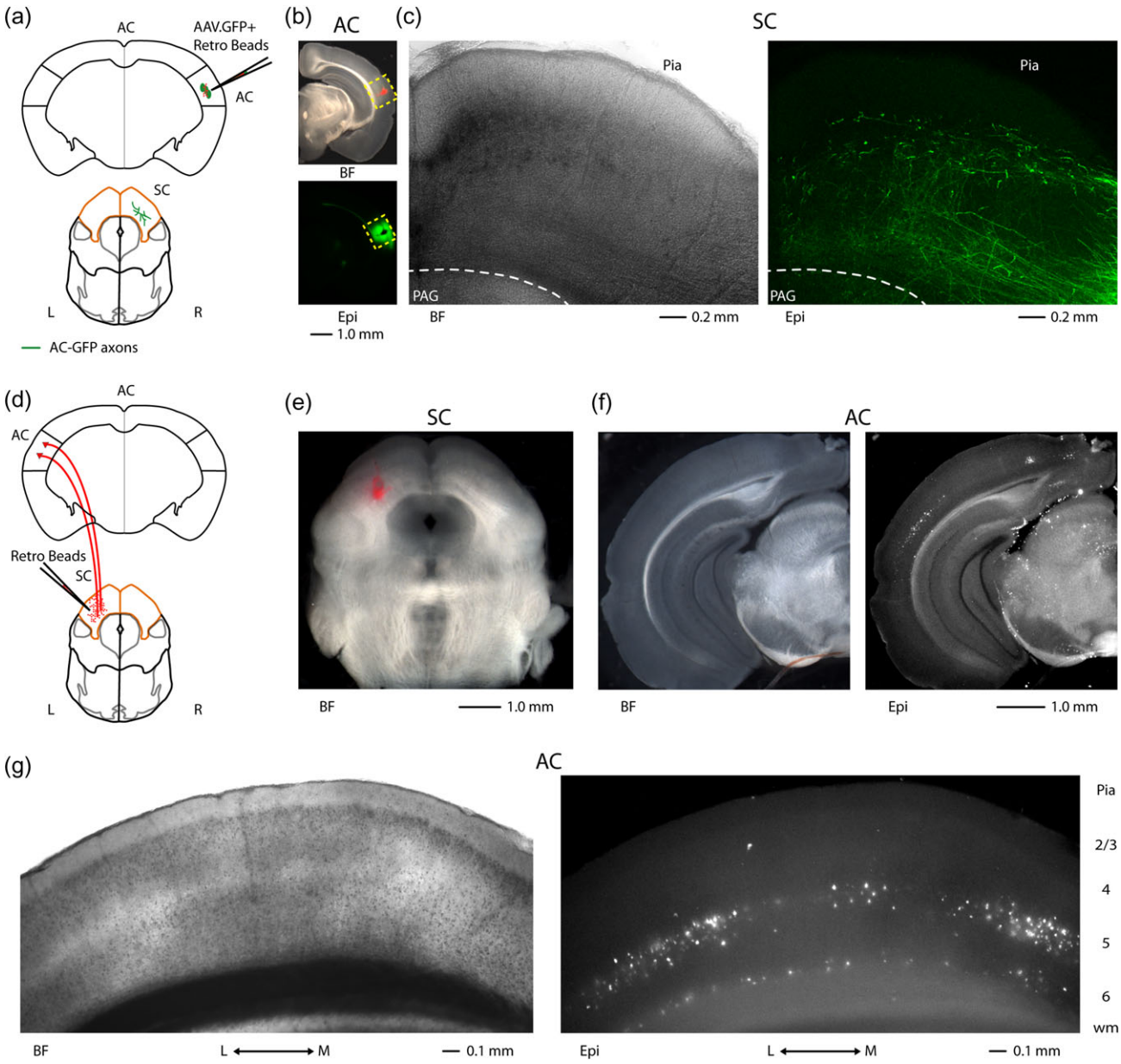

Figure 1. Auditory corticofugal projections to the SC. (*a*) Schematic depicting the injection of AAV.GFP and red RetroBeads to identify projections from the AC to the SC. (*b*) Bright-field (top) and epifluorescence (bottom) images of a slice containing the AC injection site of AAV.GFP and red RetroBeads. (*c*) Bright-field (left) and epifluorescence (right) images of a slice indicating the location GFP-labeled axons from AC neurons in the intermediate and deep layers of the SC. (*d*) Schematic depicting the injection of red RetroBeads to identify cortico-superior-collicular pyramidal neurons by anatomical retrograde labeling. (*e*) Bright-field image of a slice containing the SC injection site of red RetroBeads. (*f*) Bright-field (left) and epifluorescence (right) images of a slice containing the retrograde labeling of cortico-superior-collicular pyramidal neurons. (*g*) Bright-field (left) and epifluorescence (right) images of the laminar distribution of cortico-superior-collicular pyramidal neurons identified by anatomical retrograde labeling. Note that the long-range projecting pyramidal neurons are located in different laminae.

6: 0.8 ± 0.02 mm, $n = 11$; $P = 4.7 \times 10^{-5}$, rank-sum test) (Fig. 4*c*). Next, we determined the soma area of the layer 5 and layer 6 cortico-superior-collicular pyramidal neurons. The soma area of layer 5 cortico-superior-collicular pyramidal neurons was significantly larger compared to the layer 6 neurons (layer 5: 214.2 ± 12.4 μm^2, $n = 10$; layer 6: 123.4 ± 4.3 μm^2, $n = 11$; $P = 4.7 \times 10^{-5}$, rank-sum test) (Fig. 4*d*). We next analyzed the morphological difference between the dendrites of layer 5 and layer 6 cortico-superior-collicular pyramidal neurons. We measured the total length of their dendrites and found that layer 5 cortico-superior-collicular pyramidal neurons had a larger total length (dendritic total length layer 5: 8.721 ± 445 μm, $n = 10$; dendritic total length layer 6: 2.536 ± 171 μm, $n = 11$; $P = 4.5 \times 10^{-5}$, rank-sum test) (Fig. 4*e*). We also found that the number of dendritic branches was larger in the layer 5 cortico-superior-collicular pyramidal neurons (number of branches layer 5: 89.6 ± 3.3, $n = 10$; number of branches layer 6: 28.9 ± 1.7, $n = 11$; $P = 4.6 \times 10^{-5}$, rank-sum test) (Fig. 4*f*). Layer 5 cortico-superior-collicular pyramidal neurons also had more elaborate basal and apical dendrites compared to the layer 6 neurons. The morphological

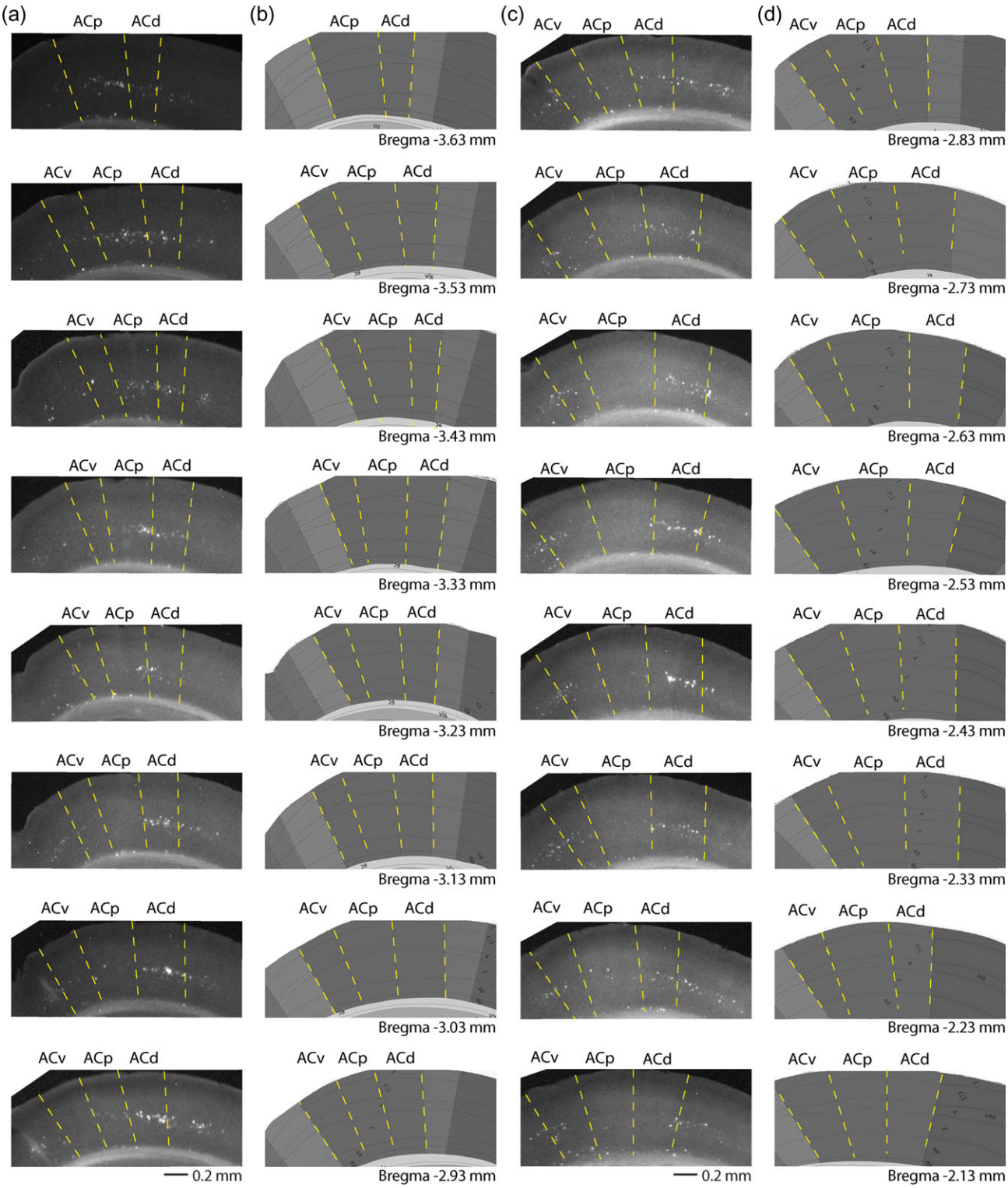

Figure 2. Areal characterization of cortico-superior-collicular neurons. (*a*) Epifluorescence images show retrogradely labeled neurons in a series of slices containing the AC. Dashed yellow lines indicate areal boundaries between the dorsal, primary, and ventral AC. (*b*) Schematic from the Allen Institute for Brain Science coronal mouse atlas which was used to reference the boundaries between the cortical areas. (*c*) Continuing in series from panel a. (*d*) Continuing in series from panel b.

differences between layer 5 and layer 6 cortico-superior-collicular pyramidal neurons were confirmed by performing Sholl analysis on individual cortico-superior-collicular pyramidal neurons (Fig. 4*g*).

These results demonstrate that the soma area and the dendritic morphologies of layer 5 and layer 6 cortico-superior-collicular pyramidal are different, which may be reflected in terms of specialized electrophysiological properties.

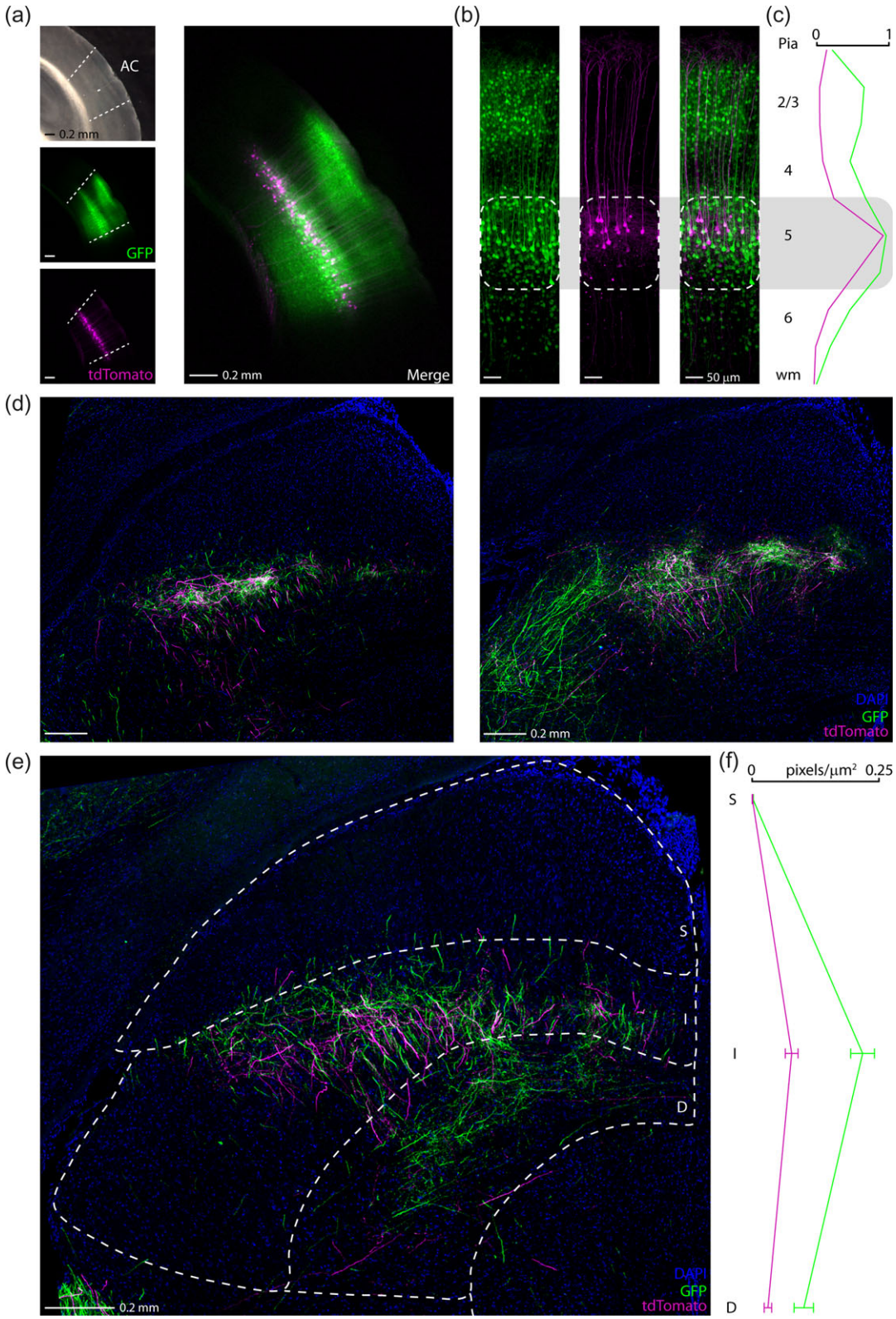

Figure 3. Distribution of auditory corticofugal projections to the SC. (*a*) Top, left: Bright-field image of a slice containing the AC injection site of AAV.GFP (pseudo-colored green in subsequent images) and AAV.tdTomato.Flex (pseudo-colored magenta in subsequent images) in the Sim1 KJ18-Cre transgenic mouse line. Middle, left: GFP fluorescence in the injection site. Bottom, left: tdTomato fluorescence in the injection site. Right: overlay of GFP and tdTomato images. (*b*) Left: Higher magnification image of GFP-expressing pyramidal neurons in the AC near the injection site. Middle: Higher magnification image of tdTomato-expressing layer 5 pyramidal neurons in the AC near the injection site. Right: Overlay of GFP and tdTomato images. The dashed box indicates the approximate layer 5 boundaries. (*c*) Normalized distribution of GFP and tdTomato expression in the AC. Fluorescence was calculated in 100 µm bins. Layer boundaries were approximated as follows: L1, 0–150 µm; L2/3, 151–375 µm; L4, 376–500 µm; L5, 501–750 µm; L6, 751–1000 µm. (*d*) Higher magnification images of GFP and tdTomato fluorescent axons in the intermediate and deep layers of the SC. (*e*) Same as in panel d, with the approximate boundaries of superficial (S), intermediate (I), and deep (D) layers of the SC indicated by dashed lines. (*f*) Normalized distribution of GFP and tdTomato expression in the superficial, intermediate, and deep layers of the SC.

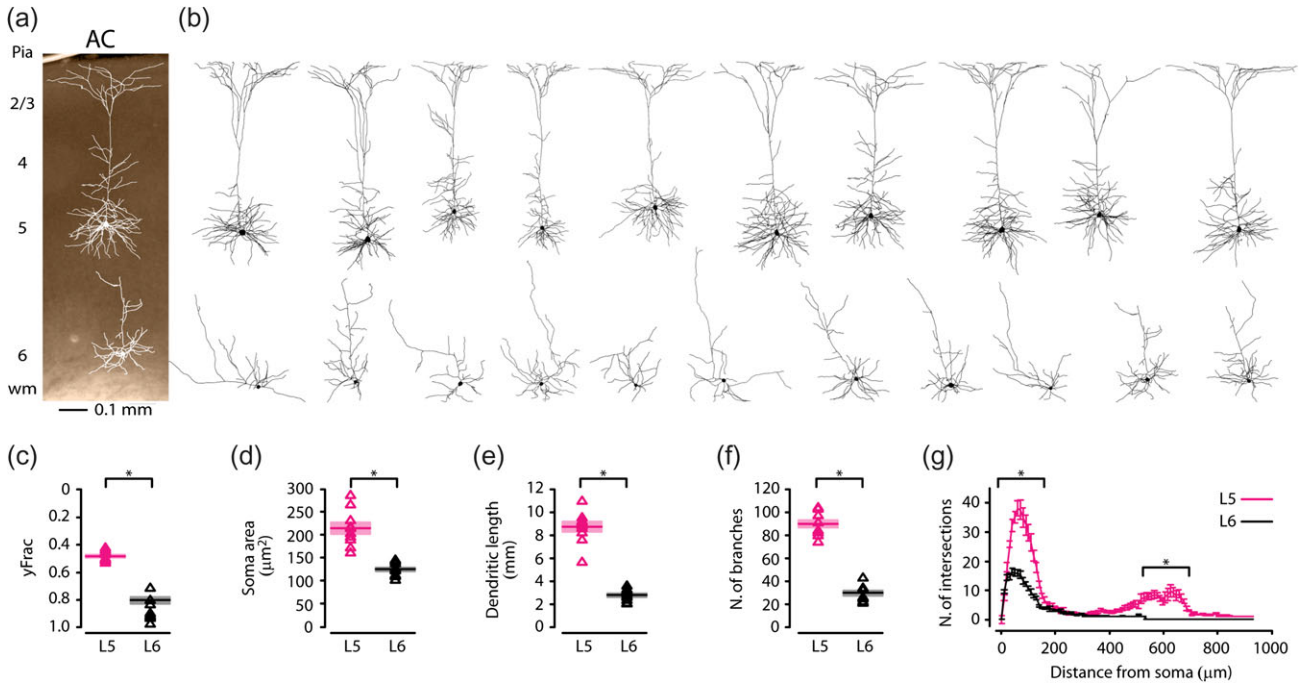

Figure 4. Anatomical characterization of cortico-superior-collicular pyramidal neurons. (*a*) Traced layer 5 and layer 6 cortico-superior-collicular pyramidal neurons superimposed on a bright-field image of a coronal brain slice illustrating the relative location of the 2 sub-classes of cortico-superior-collicular pyramidal neurons in the AC. Notice that the tuft of the layer 5 pyramidal neuron is intact, suggesting that the cutting angle of the slice is not the reason for the shorter apical dendrite of the layer 6 pyramidal neurons. (*b*) Morphological reconstructions of layer 5 (top) and layer 6 (bottom) cortico-superior-collicular pyramidal neurons. (*c*) Plot depicting the group average soma location (±s.e.m.) of layer 5 (magenta) and layer 6 (black) cortico-superior-collicular pyramidal neurons. Individual triangles mark the normalized distances from the pia to the soma for each neuron analyzed (layer 5: magenta triangles, $n = 10$, animals $n = 5$; layer 6: black triangles, $n = 11$, animals $n = 5$). (*d*) Same as in panel c, for the soma area. (*e*) Same as in panel c, for the dendritic length. (*f*) Same as in panel c, for the number of branches. (*g*) Plot shows the group average Sholl analysis (±s.e.m.) of layer 5 (magenta) and layer 6 (black) pyramidal neurons (layer 5: magenta triangles, $n = 10$, animals $n = 5$; layer 6: black triangles, $n = 11$, animals $n = 5$).

Electrophysiological Properties of Layers 5 and 6 Cortico-Superior-Collicular Pyramidal Neurons in the Mouse AC

In order to identify cortico-superior-collicular pyramidal neurons in the left AC, we injected retrograde tracers into the left SC (Fig. 1*d*–*f*). Thus, retrograde labeling allowed us to distinguish and record from visually identified layer 5 and layer 6 cortico-superior-collicular pyramidal neurons (Fig. 5*a*,*c*). Layer 5 cortico-superior-collicular pyramidal neurons typically fired in bursts during prolonged current steps while layer 6 cortico-superior-collicular pyramidal neurons exhibited regular-spiking firing, with low-to-no adaptation of APs (Fig. 5*b*,*d*). Further measurement of the intrinsic electrophysiological properties indicated that layer 5 cortico-superior-collicular pyramidal neurons were resting at a more depolarized membrane potential (layer 5: -73.9 ± 0.5 mV, $n = 26$; layer 6: -75.5 ± 0.6 mV, $n = 22$; $P = 0.028$, *t*-test), had a lower input resistance (layer 5: 104.01 ± 4.38 MΩ, $n = 26$; layer 6: 180.47 ± 8.65 MΩ, $n = 22$; $P = 1.28 \times 10^{-10}$, *t*-test), and had a slower membrane time constant (layer 5: 1.89 ± 0.11 ms, $n = 26$; layer 6: 0.97 ± 0.06 ms, $n = 22$; $P = 7.18 \times 10^{-8}$, *t*-test) compared to layer 6 cortico-superior-collicular pyramidal neurons (Fig. 5*e*).

Next, we compared the firing properties of layer 5 and layer 6 cortico-superior-collicular pyramidal neurons. Layer 5 cortico-superior-collicular pyramidal neurons had a shorter AP half-width (layer 5: 0.5 ± 0.01 ms, $n = 26$; layer 6: 0.65 ± 0.03 ms, $n = 22$; $P = 2.75 \times 10^{-5}$, *t*-test), and higher rheobase (layer 5: 165.4 ± 10.7 pA, $n = 26$; layer 6: 90.9 ± 7.1 pA, $n = 22$; $P = 1.15 \times 10^{-6}$, *t*-test), compared to layer 6 cortico-superior-collicular pyramidal neurons (Fig. 6*a*,*b*). Figure 6*c* shows an example of layer 5 and layer 6 cortico-superior-collicular pyramidal neurons' sub- and suprathreshold responses to current steps. The repetitive firing patterns of layer 5 and layer 6 cortico-superior-collicular pyramidal neurons differed in their response to depolarizing current. Layer 5 cortico-superior-collicular pyramidal neurons fired an initial burst of APs at the onset of current injections (Fig. 6*c*, magenta traces), while layer 6 cortico-superior-collicular pyramidal neurons did not (Fig. 6*c*, black traces). The initial instantaneous frequency of layer 5 cortico-superior-collicular pyramidal neurons was high (Fig. 6*d*), reflecting the initial burst firing pattern in these neurons. Moreover, the spike frequency adapted over time in layer 6 cortico-superior-collicular pyramidal neurons while it remained constant in layer 5 cortico-superior-collicular pyramidal neurons (Fig. 6*e*).

These data show that these two populations of projecting neurons in layer 5 and layer 6 of AC can be routinely differentiated by their distinct intrinsic electrophysiological properties.

Levels of I_h Expression in Layers 5 and 6 Cortico-Superior-Collicular Pyramidal Neurons

Here we test the hypothesis that layers 5 and 6 cortico-superior-collicular pyramidal neurons have different levels of I_h expression. This experiment was performed in current-clamp mode because of the limitation of voltage-clamp mode in large pyramidal neurons such as layer 5 cortico-superior-collicular pyramidal neurons (Williams and Mitchell 2008). We found that layer 5 cortico-superior-collicular pyramidal neurons displayed

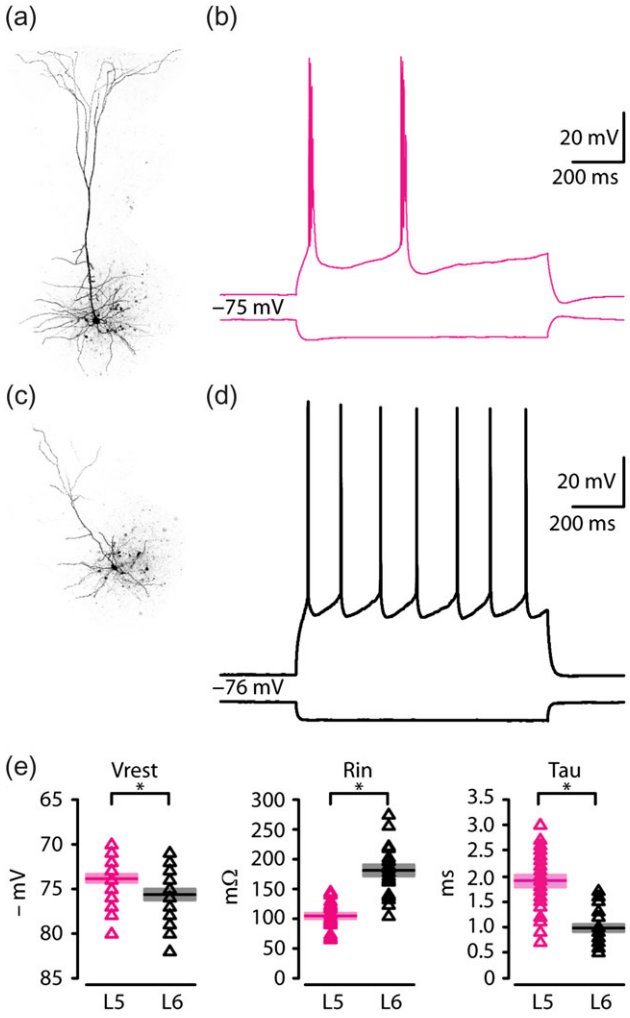

Figure 5. Electrophysiological properties of cortico-superior-collicular pyramidal neurons. (*a*) High resolution image of a biocytin-labeled layer 5 cortico-superior-collicular pyramidal neuron. (*b*) Response recorded from a layer 5 cortico-superior-collicular pyramidal neuron during injection of a hyperpolarizing current (1 s, –100 pA pulse; lower magenta trace) and a train of APs recorded during injection of a depolarizing current (1 s, 200 pA pulse; upper magenta trace). (*c*) High resolution image of a biocytin-labeled layer 6 cortico-superior-collicular pyramidal neuron. (*d*) Same as in panel c, for a layer 6 cortico-superior-collicular pyramidal neuron (black traces). (*e*) Summary plot of V_{rest}: resting membrane potential (left), R_{in}: input resistance (middle), and Tau: membrane time constant (right); recorded from layer 5 (magenta triangles, $n = 26$; animals $n = 12$) and layer 6 (black triangles, $n = 22$; animals $n = 8$) cortico-superior-collicular pyramidal neurons, including group averages (±s.e.m.).

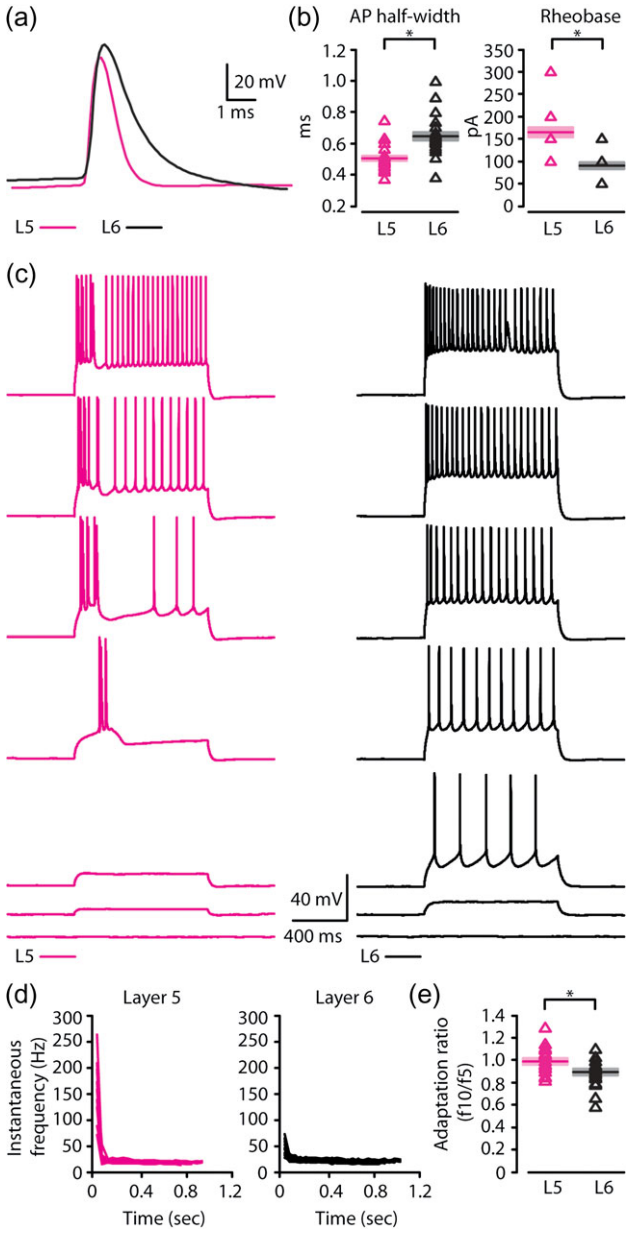

Figure 6. AP properties of cortico-superior-collicular pyramidal neurons. (*a*) Example of AP recorded from a layer 5 (magenta trace) and a layer 6 (black trace) cortico-superior-collicular pyramidal neurons. (*b*) Summary plot of AP half-width: AP half-width (left), and Rheobase: the smallest current step evoking an AP (right); recorded from layer 5 (magenta triangles, $n = 26$; animals $n = 12$) and layer 6 (black triangles, $n = 22$; animals $n = 8$) cortico-superior-collicular pyramidal neurons, including group averages (±s.e.m.). (*c*) Representative firing of layer 5 (magenta traces) and layer 6 (black traces) cortico-superior-collicular pyramidal neurons in response to increasing depolarizing current (0–300 pA, 50 pA increments). (*d*) Instantaneous firing frequency as a function of time for layer 5 (magenta triangles, $n = 26$; animals $n = 12$) and layer 6 (black triangles, $n = 22$; animals $n = 8$) cortico-superior-collicular pyramidal neurons. Initial instantaneous firing frequency is higher for layer 5 cortico-superior-collicular pyramidal neurons, which indicates bursts of APs. (*e*) Summary plot of spike frequency adaptation (f_{10}/f_5) from layer 5 (magenta triangles, $n = 26$; animals $n = 12$) and layer 6 (black triangles, $n = 22$; animals $n = 8$) cortico-superior-collicular pyramidal neurons, including group averages (±s.e.m.).

prominent "sag" of the membrane potential compared to the layer 6 neurons (layer 5: 16.1 ± 0.8%, $n = 28$; layer 6: 5.0 ± 1.2%, $n = 22$; $P = 1.6 \times 10^{-7}$, rank-sum test) (Fig. 7*a–d*). Generally, sag is a feature of I_h, but may also be attributable to other voltage-dependent conductances (Stafstrom et al. 1982). However, in our experiments, bath application of ZD7288 (an I_h channel blocker) abolished sag in layer 5 cortico-superior-collicular pyramidal neurons (layer 5 pre-ZD7288 sag: 15.6 ± 2.1%, $n = 7$; layer 5 post-ZD7288 sag: 2.0 ± 0.3%, $n = 7$; $P = 5.8 \times 10^{-4}$, rank-sum test) (Fig. 8*a–d*). Additionally, input resistance in these neurons increased after bath application of ZD7288 (layer 5 pre-ZD7288 R_{in}: 93.8 ± 7.5 mΩ, $n = 7$; layer 5 post-ZD7288 R_{in}: 124.8 ± 9.6 mΩ, $n = 7$; $P = 0.0157$, rank-sum test) (Fig. 8*e*). Similarly, bath application of ZD7288 reduced the sag in layer 6 cortico-superior-collicular pyramidal neurons, already significantly smaller than the sag in layer 5 cortico-superior-collicular pyramidal neurons ($P = 1.6 \times 10^{-7}$, rank-sum test; Fig. 7*a–d*), but

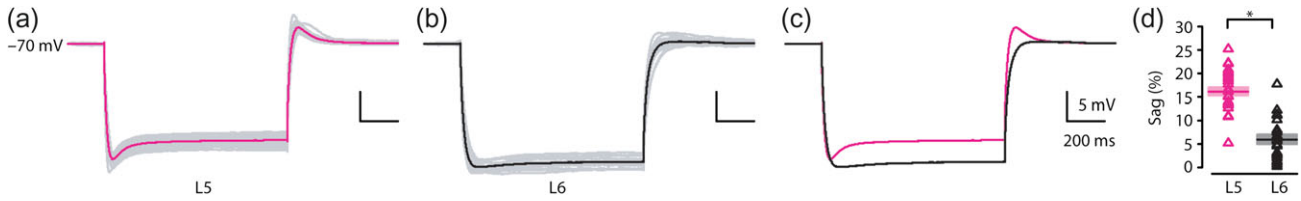

Figure 7. Difference in membrane potential sag in layer 5 and layer 6 cortico-superior-collicular pyramidal neurons. (*a*) Plot of membrane potential sag recorded from layer 5 cortico-superior-collicular pyramidal neurons (gray traces, $n = 26$; animals $n = 12$), including group averages (magenta trace). (*b*) Plot of membrane potential sag recorded from layer 6 cortico-superior-collicular pyramidal neurons (gray traces, $n = 21$; animals $n = 8$), including group averages (black trace). (*c*) Overlay of average membrane potential sag in layer 5 (magenta trace) and layer 6 (black trace). (*d*) Summary plot of membrane potential sag recorded from layer 5 (magenta triangles, $n = 26$; animals $n = 12$) and layer 6 (black triangles, $n = 21$; animals $n = 8$) cortico-superior-collicular pyramidal neurons, including group averages (±s.e.m.).

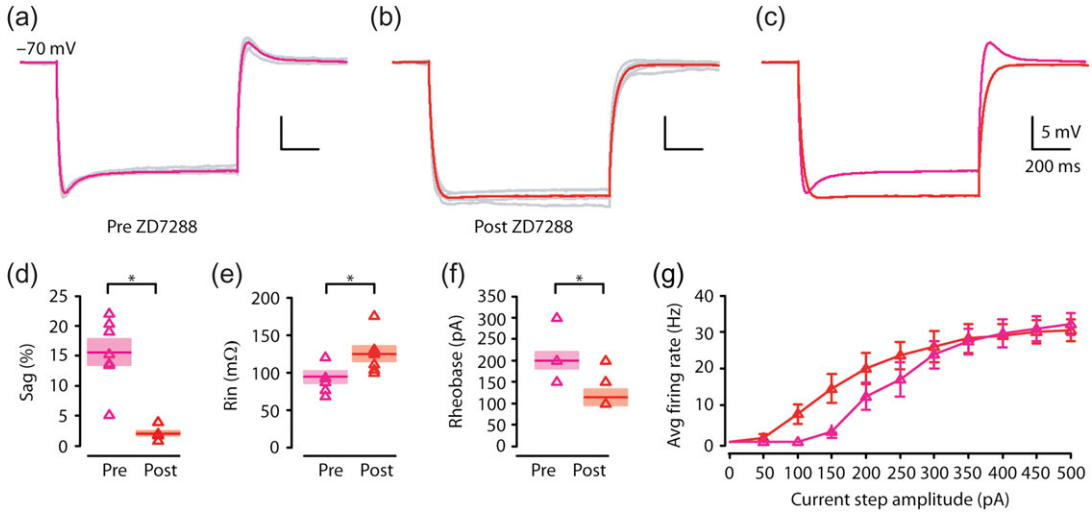

Figure 8. I_h-dependent membrane potential sag in layer 5 cortico-superior-collicular pyramidal neurons. (*a*) Plot of membrane potential sag recorded from layer 5 cortico-superior-collicular pyramidal neurons before bath application of ZD7288 (gray traces, $n = 7$; animals $n = 5$), including group averages (magenta trace). (*b*) Same as panel a, after bath application of ZD7288 (gray traces, $n = 7$; animals $n = 5$), including group averages (red trace). (*c*) Overlay of average membrane potential sag in layer 5 pre- (magenta trace) and post-ZD7288 bath application (red trace). (*d*) Summary plot of membrane potential sag recorded from layer 5 cortico-superior-collicular pyramidal neurons pre- (magenta triangles, $n = 7$; animals $n = 5$) and post-ZD7288 bath application (red triangles, $n = 7$; animals $n = 5$), including group averages (±s.e.m.). (*e*) Summary plot of R_{in}: input resistance recorded from layer 5 pre-ZD7288 (magenta triangles, $n = 7$; animals $n = 5$) and layer 5 post-ZD7288 (red triangles, $n = 7$; animals $n = 5$) cortico-superior-collicular pyramidal neurons, including group averages (±s.e.m.). (*f*) Summary plot of Rheobase recorded from layer 5 pre-ZD7288 (magenta triangles, $n = 7$; animals $n = 5$) and layer 5 post-ZD7288 (red triangles, $n = 7$; animals $n = 5$) cortico-superior-collicular pyramidal neurons, including group averages (±s.e.m.). (*g*) Summary plot F/I: frequency–current response curve recorded from layer 5 pre-ZD7288 (magenta triangles, $n = 7$; animals $n = 5$) and layer 5 post-ZD7288 (red triangles, $n = 7$; animals $n = 5$) cortico-superior-collicular pyramidal neurons, including group averages (±s.e.m.).

this reduction did not reach statistical significance indicating that these neurons express low level of I_h (layer 6 pre-ZD7288 sag: 4.6 ± 1.3%, $n = 6$; layer 6 post-ZD7288 sag: 0.9 ± 0.2%, $n = 6$; $P = 0.0649$, rank-sum test; data not shown).

In order to explore potential mechanisms of I_h regulation of firing patterns, we next compared the rheobase in layer 5 cortico-superior-collicular pyramidal neurons pre- and post-ZD7288. After I_h was blocked by bath application of ZD7288, the rheobase decreased in the layer 5 cortico-superior-collicular pyramidal neurons (layer 5 pre-ZD7288 rheobase: 200 ± 18.9 pA, $n = 7$; layer 5 post-ZD7288 rheobase: 114 ± 18 pA, $n = 7$; $P = 0.0128$, rank-sum test) (Fig. 8*f*). To further investigate this effect of I_h, we generated frequency–current (F/I) response curves for layer 5 cortico-superior-collicular pyramidal neurons pre- and post-ZD7288. We found that layer 5 cortico-superior-collicular pyramidal neurons post-ZD7288 (no sag) compared to pre-ZD7288 (with sag) had F/I curves that were shifted to the left and almost linear for small amplitude current injections (Fig. 8*g*).

These results are indicative that high expression of I_h is a characteristic property of layer 5 cortico-superior-collicular pyramidal neurons.

Effect of I_h on Synaptic Integration and Resonance in Layers 5 and 6 Cortico-Superior-Collicular Pyramidal Neurons

Differences in levels of I_h expression should affect subthreshold synaptic integration. To test this, and to quantify the efficacy of temporal summation, we injected a train of 5 EPSP-like waveforms at 20 Hz (αEPSPs) into the soma via the patch pipette (Fig. 9*a*). By using this stimulus frequency, temporal summation of αEPSPs was minimal in layer 5 cortico-superior-collicular pyramidal neurons but robust in layer 6 cortico-superior-collicular pyramidal neurons. Temporal summation was increased in layer 5 cortico-superior-collicular pyramidal neurons by bath application of ZD7288 (Fig. 9*a*,*b*). The finding that αEPSPs leads to large temporal summation in layer 6 but not layer 5 cortico-superior-collicular pyramidal neurons suggested the possibility that these neurons differentially integrate excitatory synaptic inputs. To test this hypothesis, we investigated the effect of 20 Hz presynaptic stimulation on monosynaptic excitatory inputs to layer 5 and layer 6 cortico-superior-collicular pyramidal neurons. For this experiment, we electrically stimulated the

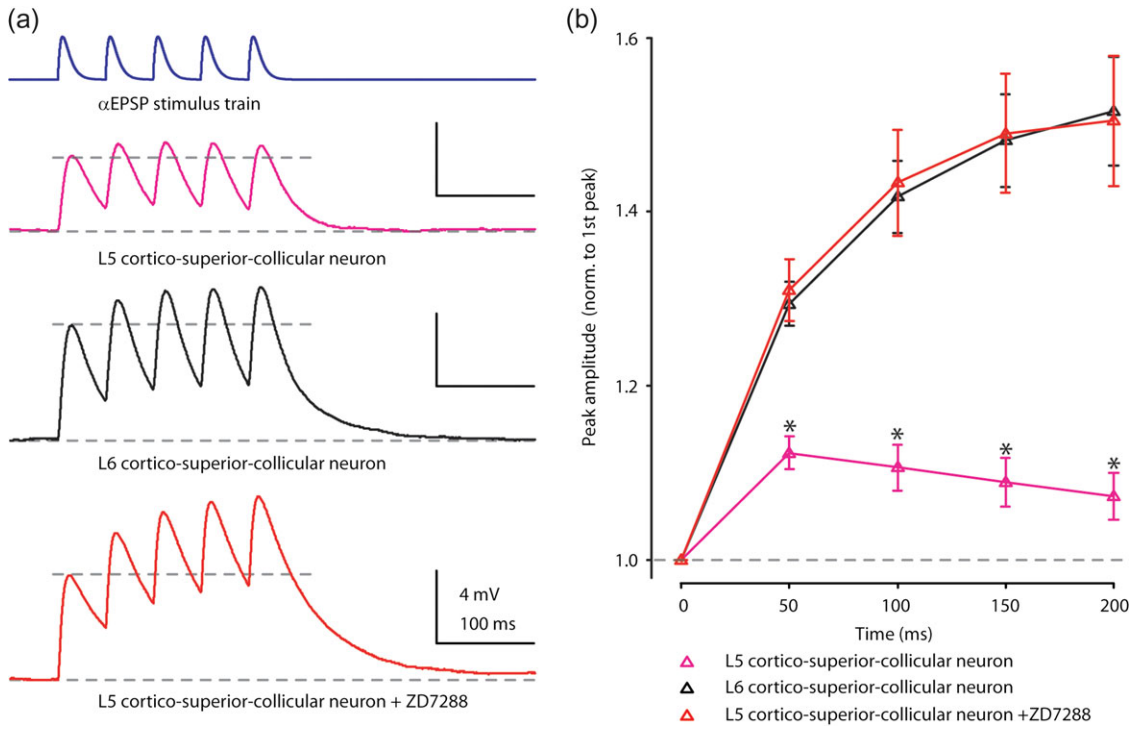

Figure 9. I_h influences the temporal summation of artificial EPSCs in layer 5 but not in layer 6 cortico-superior-collicular pyramidal neurons. (*a*) Example responses to a 20 Hz train of 5 EPSC-like waveforms (top) recorded from layer 5 (magenta trace), layer 6 (black trace) cortico-superior-collicular pyramidal neurons. Layer 5 cortico-superior-collicular pyramidal neurons show increased temporal summation after bath application of ZD7288 (red trace). Dashed gray lines indicate the amplitude of the first recorded response as a baseline. (*b*) Average plot of peak responses to a train of EPSC-like waveforms normalized to first peak (layer 5 pre-ZD7288: magenta triangles, $n = 26$; animals $n = 12$; layer 6: black triangles, $n = 21$; animals $n = 8$; layer 5 post-ZD7288: red triangles, $n = 7$; animals $n = 5$), including group averages (±s.e.m.).

cortex by placing a stimulating electrode between layer 5 and layer 6 of the AC while recording EPSCs from layer 5 and layer 6 cortico-superior-collicular pyramidal neurons (Fig. 10*a*). It is important to note that electrical stimulation of the AC can also lead to the firing of GABAergic neurons. However, we assume that by applying a command potential −70 mV (the calculated reversal potential for GABAergic inhibitory conductance) we can separate the majority of the excitatory inputs (EPSCs) from the inhibitory. By using this stimulus frequency, temporal summation of EPSCs was minimal in layer 5 cortico-superior-collicular pyramidal neurons but robust in layer 6 neurons (Fig. 10*b*,*c*). These data indicate that I_h, when activated by current injection at the soma level, strongly attenuates the summation of αEPSPs in layer 5 cortico-superior-collicular pyramidal neurons.

Previous studies have shown that I_h controls neuronal resonance (Hutcheon and Yarom 2000; Narayanan and Johnston 2007; Shin et al. 2008; Dembrow et al. 2010; Sheets et al. 2011). Next, we determined how the I_h can influence the dynamic properties of layers 5 and 6 cortico-superior-collicular pyramidal neurons by measuring their resonance frequency. To measure the resonance frequency of layers 5 and 6 cortico-superior-collicular pyramidal neurons we delivered a subthreshold chirp stimulus (frequency-swept sinusoids ranging linearly between 0–20 Hz over a period of time of 20 s) (Fig. 11*a*, top) via the patch pipette and calculated the impedance amplitude profiles (ZAPs). Layer 5 cortico-superior-collicular pyramidal neurons resonated in the theta frequency range, with a peak centered at ~3 Hz, while layer 6 cortico-superior-collicular pyramidal neurons declined monotonically with the frequency (Fig. 11*a*,*b*). Blocking I_h in layer 5 cortico-superior-collicular pyramidal neurons by bath application of ZD7288 abolished their resonance frequency, and their post-ZD7288 ZAPs resembled those of layer 6 cortico-superior-collicular pyramidal neurons (layer 5 resonant frequency: 3.0 ± 0.2 Hz, $n = 28$; layer 6 resonant frequency: 0.95 ± 0.005 Hz, $n = 19$; layer 5 post-ZD7288 resonant frequency: 0.8 ± 0.1 Hz, $n = 7$; layer 5 vs. layer 6: $P = 4.3 \times 10^{-8}$, rank-sum test; layer 5 pre- vs. post-ZD7288: $P = 5.8 \times 10^{-4}$, rank-sum test) (Fig. 11*b*).

Discussion

This study reveals that AC, including the primary AC, sends excitatory/glutamatergic projections to the intermediate and deep layers of the SC via layers 5 and 6 pyramidal neurons (Fig. 12). Furthermore, it also identifies a specific function in which layer 5 cortico-superior-collicular pyramidal neurons act as bandpass filters, resonating with a broad peak at ~3 Hz, whereas layer 6 cortico-superior-collicular pyramidal neurons act as low-pass filters. This dissimilarity can be ascribed to differences in their levels of I_h expression.

Auditory Corticofugal Projections to the SC

Previous studies of corticofugal projections to the SC have mainly been focused on the input coming from the visual cortex (for review see, Wurtz and Albano 1980). In these studies, the function of corticofugal projections have been determined both at a physiological and a behavioral level (Stein 1978; Clemo and Stein 1986; Meredith and Clemo 1989; Wallace et al. 1993; Jiang et al. 2002; Alvarado et al. 2007). Most recently, studies from cat (Chabot et al. 2013) and ferret (Bajo et al. 2010) have shown that the cortical inputs to the SC originate in areas outside of the primary AC. In the cat, this area is the anterior

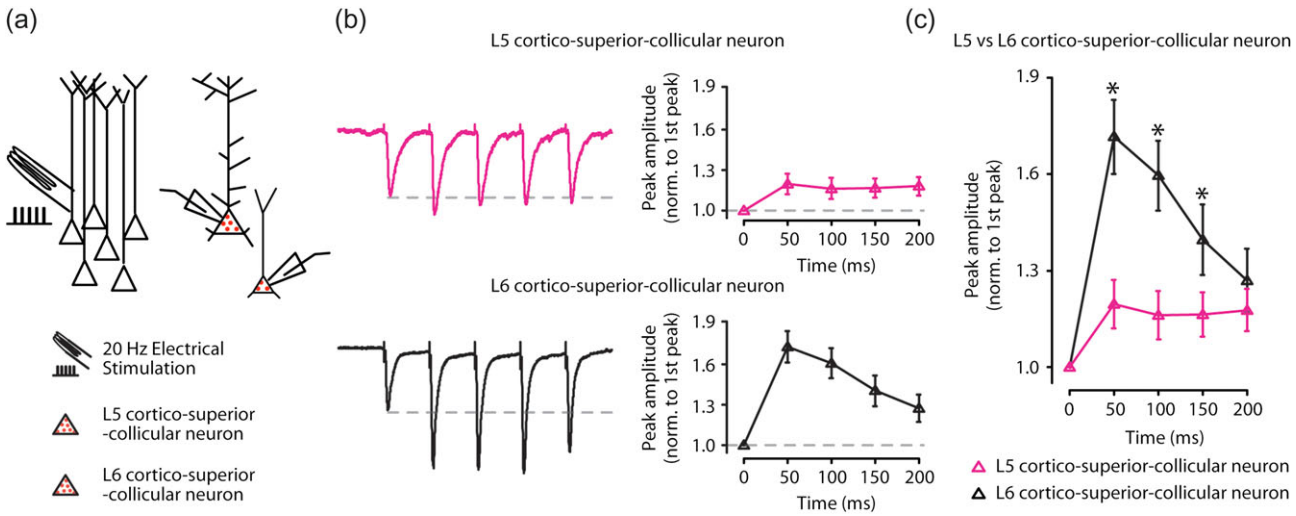

Figure 10. Temporal summation of EPSCs in layer 5 but not in layer 6 cortico-superior-collicular pyramidal neurons. (*a*) Experimental paradigm for electrical stimulation of the AC while recording excitatory synaptic inputs from layer 5 and layer 6 cortico-superior-collicular pyramidal neurons identified by anatomical retrograde labeling. (*b*) Example responses to a 20 Hz train of 5 electrical pulses recorded from layer 5 (top, magenta trace) and layer 6 (bottom, black trace) cortico-superior-collicular pyramidal neurons. Temporal summation of EPSCs was minimal in layer 5 cortico-superior-collicular pyramidal neurons but robust in layer 6 cortico-superior-collicular pyramidal neurons. (*c*) Average plot of peak responses to a train of EPSCs normalized to first peak (layer 5 magenta triangles, $n = 10$; animals $n = 6$; layer 6: black triangles, $n = 9$; animals $n = 6$), including group averages (±s.e.m.).

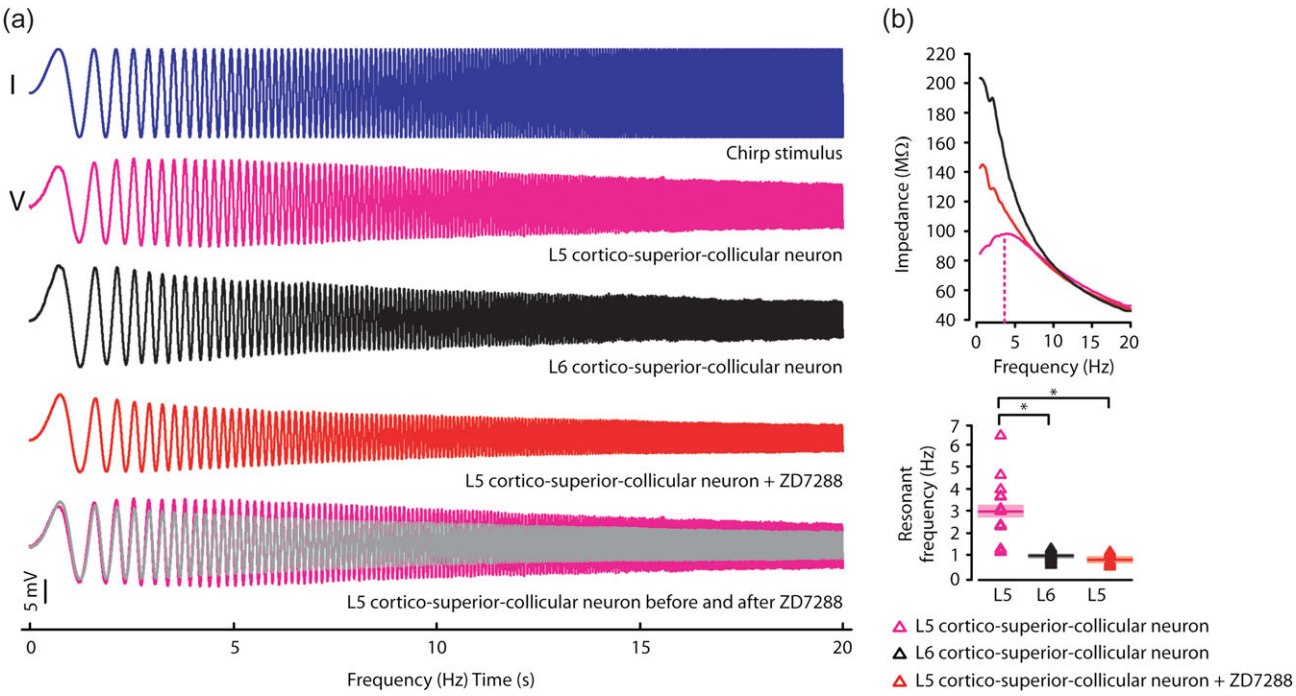

Figure 11. Resonance frequency in layer 5 and layer 6 cortico-superior-collicular pyramidal neurons is I_h-dependent. (*a*) Example of chirp current stimulus (I, top) and chirp voltage (V) responses recorded from layer 5 (magenta trace), layer 6 (black trace), and layer 5 cortico-superior-collicular pyramidal neuron treated with bath application of ZD7288 (red trace). Bottom: overlaid responses of a layer 5 cortico-collicular pyramidal neurons before (magenta) and after (gray) ZD7288 bath application. (*b*) Top: Example of an impedance amplitude profile of a layer 5 (magenta trace), a layer 6 (black trace), and a layer 5 cortico-superior-collicular pyramidal neuron after ZD7288 bath application (red trace). Bottom: Summary plot of resonance frequency recorded from layer 5 (magenta triangles, $n = 28$; animals $n = 12$), layer 6 (black triangles, $n = 20$; animals $n = 8$), and layer 5 cortico-superior-collicular pyramidal neurons after ZD7288 (red triangles, $n = 7$; animals $n = 5$), including group averages (±s.e.m.).

ectosylvian sulcus, an area that heavily projects to the SC and plays an important role in multisensory integration (for review see, Stein 1998). Our findings are consistent with previous results demonstrating that both the dorsal and the ventral AC project to the SC, but we also provide evidence for a new concept in which the primary AC innervates the SC as well. Additionally, we found that these cortico-superior-collicular projections originate in both layers 5 and 6 of the AC, in contrast with previous studies showing that these projections mainly originated in layer 5 (Bajo et al. 2010; Butler et al. 2016).

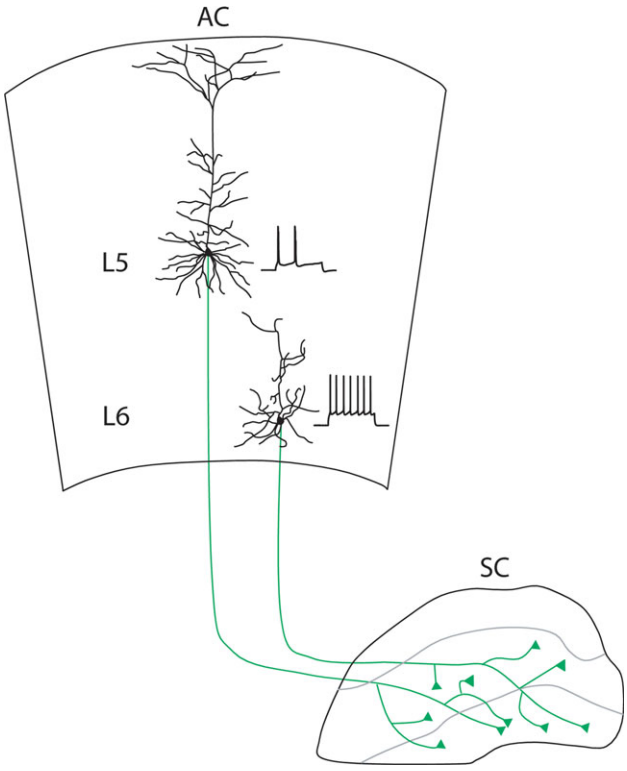

Figure 12. Schematic depicting corticofugal projections from layers 5 and 6 pyramidal neurons in the AC to the SC. Green lines: excitatory inputs from layers 5 and 6 cortico-superior-collicular pyramidal neurons.

We also found morphological dendritic differences between the layers 5 and 6 cortico-superior-collicular pyramidal neurons, suggesting that these two cell-types influence the AC-SC pathway according to their specialized cortical circuit organization.

Layer-specific Expression of I_h

In the cortex, HCN channels are primarily located in pyramidal neuron distal dendrites (for review see, Johnston and Narayanan 2008; Shah et al. 2010). Dendritic HCN channels are able to lower membrane resistance and depolarize the membrane resting potential by providing a leakage path for the current flow that can modify the time course of EPSPs. Particularly, the dendritic HCN channels, by decreasing the membrane time constant, increases the decay of the distal EPSPs. As a result, inhibition of HCN channels increases the excitability of dendrites and synaptic potential summation regardless of the membrane potential being hyperpolarized (for review see, Robinson and Siegelbaum 2003).

Our electrophysiological and pharmacological experiments have indicated that layer 5 cortico-superior-collicular pyramidal neurons express high levels of I_h, whereas layer 6 cortico-superior-collicular pyramidal neurons do not. Layer 5 cortico-superior-collicular pyramidal neurons also exhibited more resonance, sag, and less temporal summation, while the pharmacological blockade of I_h with the I_h channel blocker ZD7288 abolishes these properties.

It is well established that the expression of I_h is cell-specific and it is related primarily to their differential long-range axonal target (Kasper et al. 1994; Christophe et al. 2005; Brown and Hestrin 2009; Dembrow et al. 2010; Sheets et al. 2011; Joshi et al. 2015; Rock and Apicella 2015). However, our data expands on this knowledge and demonstrates that pyramidal neurons located in different cortical laminae but projecting to the same target may have different levels of I_h expression.

The contribution of I_h to the dynamic properties of layers 5 and 6 cortico-superior-collicular pyramidal neurons may be distinct for several reasons. One possibility is that the perisomatic level of I_h is able to cause the layer 5 but not the layer 6 cortico-superior-collicular pyramidal neurons to resonate. However, difference in I_h current may not be dependent exclusively on the perisomatic level of I_h. Different HCN channels with varied subunit compositions contribute to the overall expression of I_h (Santoro et al. 2000; Chen et al. 2001; Ulens and Tytgat 2001) and some previous studies have shown that levels of HCN channel subunit expression are projection target specific (Santoro et al. 2000; Sheets et al. 2011). In addition, the contribution of I_h to the dynamic properties of layers 5 and 6 cortico-superior-collicular pyramidal neurons measured at the soma level can be explained by different levels of I_h expression along the dendrites. It has been demonstrated in previous studies that I_h currents are typically enriched in the dendrites of pyramidal neurons (Magee 1998; Williams and Stuart 2000; Kole et al. 2006) and measurement of resonance frequency is sensitive to attenuation along the dendrites (Narayanan and Johnston 2007; Williams and Mitchell 2008). In this study, our recordings are made at the somatic level. For this reason, we cannot exclude the possibility that the difference in the dynamic properties of layers 5 and 6 cortico-superior-collicular pyramidal neurons that we have observed may be limited to the perisomatic region. Determining the dendritic distribution of HCN channels in layers 5 and 6 cortico-superior-collicular pyramidal neurons remains an important question for future studies.

One more important aspect of the I_h is that is strongly regulated by neuromodulation (Biel et al. 2009). Future studies, in order to better understand the effect of up and/or downregulation of I_h of the cortico-superior-collicular pathways, will be to distinguish how dopaminergic, serotonergic, and noradrenergic projections differentially influence the layer 5 cortico-superior-collicular pyramidal neurons at both circuit and behavioral levels.

Layers 5 and 6 Cortico-Superior-Collicular Pyramidal Neurons: From Circuits to Behavior

Lesions of the AC in the ferret produce deficits in orienting behavior (Nodal et al. 2010). Additionally, it has been shown that manipulation of the SC in monkeys plays an important role in making perceptual decisions (Lovejoy and Krauzlis 2010), a function that is normally thought to be cortex-dependent. These findings may highlight an important aspect of how corticofugal projections modulate the neuronal response of the SC, in that changes in the corticofugal projections from the AC to the SC could disrupt normal sound-driven orienting behavior. Our findings, that cortico-superior-collicular pyramidal neurons are located in both layers 5 and 6 of the AC and have different anatomical and electrophysiological properties, suggest these two sub-classes of projection neurons could be involved in different functions.

Previous studies have shown that layer 5 pyramidal neurons have different morphology, connections (for review see, Winer et al. 1998; Winer 2006), and exhibit different responses to auditory stimuli compared to layer 6 pyramidal neurons (Sugimoto et al. 1997; Hromadka et al. 2008; Atencio and Schreiner 2016; for review see Linden and Schreiner 2003; Wu et al. 2011). In particular, Sakata and Harris (2009) observed that layer 5 thick-tufted

neurons (such as layer 5 cortico-superior-collicular pyramidal neurons) exhibit a greater response to sound stimulation compared to other pyramidal neurons in the AC. A more recent finding in layer 5 of the AC by Sun et al. (2013) suggested that intrinsic-bursting pyramidal neurons (such as layer 5 cortico-superior-collicular-like pyramidal neurons) have spectrally and temporally broader synaptic integration than regular-spiking pyramidal neurons (such as layer 6 cortico-superior-collicular-like pyramidal neurons). Layer 5 intrinsic-bursting pyramidal neurons (such as layer 5 cortico-superior-collicular-like pyramidal neurons) show sustained firing in vivo, which is in agreement with our results demonstrating that layer 5 cortico-superior-collicular pyramidal neurons have little or no spike frequency adaptation and a narrower AP. Moreover, the bursting pattern of APs observed in the presence of excitatory and inhibitory synaptic blockers suggests that the intrinsic properties of layer 5 cortico-superior-collicular pyramidal neurons may contribute to the sustained response of layer 5 intrinsic-bursting neurons to auditory stimuli (Sun et al. 2013). Stimulation of the AC enhances neuronal response of midbrain regions, such as the inferior colliculus via corticofugal projections, at the preferred frequency of their tuning curve and inhibits these regions at frequencies lower or higher than the preferred frequency (Sun et al. 1996; Yan and Suga 1996). Moreover, given that corticofugal projections, by shaping the response of the inferior collicular neurons, promote sound localization learning (Bajo et al. 2010), our results invite speculation that sustained activity in the layer 5 cortico-superior-collicular pathway may play an important role in inducing learning of acoustically driven orientation behavior.

Anatomical studies have revealed three main classes of pyramidal neurons located in layer 6 of the neocortex (for review see Thomson 2010). Corticothalamic pyramidal neurons are estimated to constitute ~50% of the entire layer 6 neuronal population and provide feedback projections with small terminals exclusively to the thalamus (Ojima 1994; Prieto and Winer 1999; Rouiller and Welker 2000; Winer et al. 2005; Takayanagi and Ojima 2006; Llano and Sherman 2008). The rest of the layer 6 neurons are typically classified as ~30–40% corticocortical pyramidal neurons and ~15% GABAergic neurons (Gilbert and Kelly 1975; Zhang and Deschenes 1997; Kumar and Ohana 2008). Our results reveal that there exists another class of layer 6 pyramidal neurons, projecting directly to the SC, which also contribute to descending auditory corticofugal projections.

In a recent study in rodents, Zhou et al. (2010) observed two categories of sound-evoked spike responses in the layer 6 of the AC. In particular, they revealed that the majority of layer 6 pyramidal neurons do not respond to sound stimulation while a smaller fraction of layer 6 pyramidal neurons, which are directly driven by thalamic input, respond with a robust sound-evoked spike response. It is yet to be determined whether layer 6 cortico-superior-collicular pyramidal neurons will belong to the class of layer 6 pyramidal neurons which do or do not respond to sound stimuli in vivo. To address this possibility, future studies are required to examine how sound stimuli affect the dynamic properties of excitatory and inhibitory inputs onto layer 6 cortico-superior-collicular pyramidal neurons. However, our results demonstrate that layer 6 cortico-superior-collicular pyramidal neurons have spike frequency adaptation and a broad AP, suggesting that these neurons may exhibit a more phasic response to auditory stimuli. Therefore, layer 6 cortico-superior-collicular pyramidal neurons, by responding more effectively to new acoustic stimulation, could preferentially trigger behavior related to novelty, such as flight behavior (Liang et al. 2015; Xiong et al. 2015; Zingg et al. 2017).

As proposed by Reichova and Sherman (2004), glutamatergic inputs can be divided in drivers (first large EPSCs that show evidence of paired-pulse depression) and modulators (first small EPSCs that show evidence of paired-pulse facilitation). Our findings, that cortico-superior-collicular pyramidal neurons located in both layers 5 and 6 of the AC possibly innervate the same layers of the SC together with their different electrophysiological properties invites speculation that their glutamatergic inputs may provide different inputs to the same layers of the SC with distinct short-term plasticity mechanisms (for review see, Lee and Sherman 2010). These distinctive driver and modulator glutamatergic inputs may serve separate functions in cortico-superior-collicular circuits which may be engaged differently during defensive–like and/or orienting behavior.

An important question for future studies, in order to better understand the effect of cortico-superior-collicular pathways on the SC, will be to distinguish how each cortical area, cortical layer, and cell-types affect different SC outputs at both circuit and behavioral levels.

Conclusion

The present results demonstrate a direct projection from Layers 5 and 6 pyramidal neurons from AC, including the primary auditory cortex, to the SC. Layers 5 and 6 cortico-superior-collicular pyramidal neurons are unique subclasses of neurons characterized by different anatomical, electrophysiological, and synaptic properties. Furthermore, these results can help in designing experiments to investigate the link between the 2 layer-specific subclasses of projection neurons to the SC that may serve separate functions in cortico-superior-collicular circuits and that may be engaged differently during defensive-like and/or orienting behavior.

Funding

This work was supported by the National Institute of General Medical Sciences Grant 1SC1GM122645 (A.j.A.).

Notes

We are indebted to M. Scanziani for advice, encouragement and comments on the manuscript. We are grateful to G. Gaufo and K. Hanson for help with confocal imaging. *Conflict of Interest*: None declared.

References

Alvarado JC, Stanford TR, Vaughan JW, Stein BE. 2007. Cortex mediates multisensory but not unisensory integration in superior colliculus. J Neurosci. 27:12775–12786.

Atencio CA, Schreiner CE. 2016. Functional congruity in local auditory cortical microcircuits. Neuroscience. 316:402–419.

Bajo VM, King AJ. 2012. Cortical modulation of auditory processing in the midbrain. Front Neural Circuits. 6:114.

Bajo VM, Nodal FR, Bizley JK, King AJ. 2010. The non-lemniscal auditory cortex in ferrets: convergence of corticotectal inputs in the superior colliculus. Front Neuroanat. 4:18.

Bajo VM, Nodal FR, Bizley JK, Moore DR, King AJ. 2007. The ferret auditory cortex: descending projections to the inferior colliculus. Cereb Cortex. 17:475–491.

Bajo VM, Nodal FR, Moore DR, King AJ. 2010. The descending corticocollicular pathway mediates learning-induced auditory plasticity. Nat Neurosci. 13:253–260.

Biel M, Wahl-Schott C, Michalakis S, Zong X. 2009. Hyperpolarization-activated cation channels: from genes to function. Physiol Rev. 89:847–885.

Brown SP, Hestrin S. 2009. Intracortical circuits of pyramidal neurons reflect their long-range axonal targets. Nature. 457: 1133–1136.

Butler BE, Chabot N, Lomber SG. 2016. A quantitative comparison of the hemispheric, areal, and laminar origins of sensory and motor cortical projections to the superior colliculus of the cat. J Comp Neurol. 524:2623–2642.

Chabot N, Mellott JG, Hall AJ, Tichenoff EL, Lomber SG. 2013. Cerebral origins of the auditory projection to the superior colliculus of the cat. Hear Res. 300:33–45.

Chen S, Wang J, Siegelbaum SA. 2001. Properties of hyperpolarization-activated pacemaker current defined by coassembly of HCN1 and HCN2 subunits and basal modulation by cyclic nucleotide. J Gen Physiol. 117:491–504.

Christophe E, Doerflinger N, Lavery DJ, Molnar Z, Charpak S, Audinat E. 2005. Two populations of layer v pyramidal cells of the mouse neocortex: development and sensitivity to anesthetics. J Neurophysiol. 94:3357–3367.

Clemo HR, Stein BE. 1986. Effects of cooling somatosensory cortex on response properties of tactile cells in the superior colliculus. J Neurophysiol. 55:1352–1368.

Cowie RJ, Robinson DL. 1994. Subcortical contributions to head movements in macaques. I. Contrasting effects of electrical stimulation of a medial pontomedullary region and the superior colliculus. J Neurophysiol. 72:2648–2664.

Dembrow NC, Chitwood RA, Johnston D. 2010. Projection-specific neuromodulation of medial prefrontal cortex neurons. J Neurosci. 30:16922–16937.

DesJardin JT, Holmes AL, Forcelli PA, Cole CE, Gale JT, Wellman LL, Gale K, Malkova L. 2013. Defense-like behaviors evoked by pharmacological disinhibition of the superior colliculus in the primate. J Neurosci. 33:150–155.

Diamond IT, Jones EG, Powell TP. 1969. The projection of the auditory cortex upon the diencephalon and brain stem in the cat. Brain Res. 15:305–340.

Emmenlauer M, Ronneberger O, Ponti A, Schwarb P, Griffa A, Filippi A, Nitschke R, Driever W, Burkhardt H. 2009. XuvTools: free, fast and reliable stitching of large 3D datasets. J Microsc. 233:42–60.

Ferreira TA, Blackman AV, Oyrer J, Jayabal S, Chung AJ, Watt AJ, Sjostrom PJ, van Meyel DJ. 2014. Neuronal morphometry directly from bitmap images. Nat Methods. 11:982–984.

Gilbert CD, Kelly JP. 1975. The projections of cells in different layers of the cat's visual cortex. J Comp Neurol. 163:81–105.

Hikosaka O, Wurtz RH. 1985. Modification of saccadic eye movements by GABA-related substances. I. Effect of muscimol and bicuculline in monkey superior colliculus. J Neurophysiol. 53: 266–291.

Hromadka T, Deweese MR, Zador AM. 2008. Sparse representation of sounds in the unanesthetized auditory cortex. PLoS Biol. 6:e16.

Hutcheon B, Yarom Y. 2000. Resonance, oscillation and the intrinsic frequency preferences of neurons. Trends Neurosci. 23:216–222.

Jiang W, Jiang H, Stein BE. 2002. Two corticotectal areas facilitate multisensory orientation behavior. J Cogn Neurosci. 14: 1240–1255.

Johnston D, Narayanan R. 2008. Active dendrites: colorful wings of the mysterious butterflies. Trends Neurosci. 31:309–316.

Joshi A, Middleton JW, Anderson CT, Borges K, Suter BA, Shepherd GM, Tzounopoulos T. 2015. Cell-specific activity-dependent fractionation of layer 2/3–>5B excitatory signaling in mouse auditory cortex. J Neurosci. 35:3112–3123.

Kasper EM, Larkman AU, Lubke J, Blakemore C. 1994. Pyramidal neurons in layer 5 of the rat visual cortex. I. Correlation among cell morphology, intrinsic electrophysiological properties, and axon targets. J Comp Neurol. 339:459–474.

King AJ. 2004. The superior colliculus. Curr Biol. 14:R335–R338.

King AJ, Jiang ZD, Moore DR. 1998. Auditory brainstem projections to the ferret superior colliculus: anatomical contribution to the neural coding of sound azimuth. J Comp Neurol. 390:342–365.

Kole MH, Hallermann S, Stuart GJ. 2006. Single Ih channels in pyramidal neuron dendrites: properties, distribution, and impact on action potential output. J Neurosci. 26:1677–1687.

Kumar P, Ohana O. 2008. Inter- and intralaminar subcircuits of excitatory and inhibitory neurons in layer 6a of the rat barrel cortex. J Neurophysiol. 100:1909–1922.

Lee CC, Sherman SM. 2010. Drivers and modulators in the central auditory pathways. Front Neurosci. 4:79.

Liang F, Xiong XR, Zingg B, Ji XY, Zhang LI, Tao HW. 2015. Sensory cortical control of a visually induced arrest behavior via corticotectal projections. Neuron. 86:755–767.

Linden JF, Schreiner CE. 2003. Columnar transformations in auditory cortex? A comparison to visual and somatosensory cortices. Cereb Cortex. 13:83–89.

Llano DA, Sherman SM. 2008. Evidence for nonreciprocal organization of the mouse auditory thalamocortical-corticothalamic projection systems. J Comp Neurol. 507:1209–1227.

Lomber SG, Payne BR, Cornwell P. 2001. Role of the superior colliculus in analyses of space: superficial and intermediate layer contributions to visual orienting, auditory orienting, and visuospatial discriminations during unilateral and bilateral deactivations. J Comp Neurol. 441:44–57.

Longair MH, Baker DA, Armstrong JD. 2011. Simple Neurite Tracer: open source software for reconstruction, visualization and analysis of neuronal processes. Bioinformatics. 27:2453–2454.

Lovejoy LP, Krauzlis RJ. 2010. Inactivation of primate superior colliculus impairs covert selection of signals for perceptual judgments. Nat Neurosci. 13:261–266.

Magee JC. 1998. Dendritic hyperpolarization-activated currents modify the integrative properties of hippocampal CA1 pyramidal neurons. J Neurosci. 18:7613–7624.

Malmierca MS, Ryugo DK. 2011. Descending connections of auditory cortex to the midbrain and brain stem. In: Winer JA, Schreiner E, editors. The auditory cortex. New York Dordrecht Heidelberg London: Springer. p. 189–208.

McHaffie JG, Stein BE. 1982. Eye movements evoked by electrical stimulation in the superior colliculus of rats and hamsters. Brain Res. 247:243–253.

Meredith MA, Clemo HR. 1989. Auditory cortical projection from the anterior ectosylvian sulcus (Field AES) to the superior colliculus in the cat: an anatomical and electrophysiological study. J Comp Neurol. 289:687–707.

Narayanan R, Johnston D. 2007. Long-term potentiation in rat hippocampal neurons is accompanied by spatially widespread changes in intrinsic oscillatory dynamics and excitability. Neuron. 56:1061–1075.

Nodal FR, Doubell TP, Jiang ZD, Thompson ID, King AJ. 2005. Development of the projection from the nucleus of the brachium of the inferior colliculus to the superior colliculus in the ferret. J Comp Neurol. 485:202–217.

Nodal FR, Kacelnik O, Bajo VM, Bizley JK, Moore DR, King AJ. 2010. Lesions of the auditory cortex impair azimuthal sound localization and its recalibration in ferrets. J Neurophysiol. 103:1209–1225.

Ojima H. 1994. Terminal morphology and distribution of corticothalamic fibers originating from layers 5 and 6 of cat primary auditory cortex. Cereb Cortex. 4:646–663.

Oviedo HV, Bureau I, Svoboda K, Zador AM. 2010. The functional asymmetry of auditory cortex is reflected in the organization of local cortical circuits. Nat Neurosci. 13:1413–1420.

Prieto JJ, Winer JA. 1999. Layer VI in cat primary auditory cortex: Golgi study and sublaminar origins of projection neurons. J Comp Neurol. 404:332–358.

Redgrave P, Dean P, Souki W, Lewis G. 1981. Gnawing and changes in reactivity produced by microinjections of picrotoxin into the superior colliculus of rats. Psychopharmacology (Berl). 75: 198–203.

Reichova I, Sherman SM. 2004. Somatosensory corticothalamic projections: distinguishing drivers from modulators. J Neurophysiol. 92:2185–2197.

Robinson RB, Siegelbaum SA. 2003. Hyperpolarization-activated cation currents: from molecules to physiological function. Annu Rev Physiol. 65:453–480.

Rock C, Apicella AJ. 2015. Callosal projections drive neuronal-specific responses in the mouse auditory cortex. J Neurosci. 35:6703–6713.

Rock C, Zurita H, Wilson C, Apicella AJ. 2016. An inhibitory corticostriatal pathway. Elife. 5:e15890.

Rouiller EM, Welker E. 2000. A comparative analysis of the morphology of corticothalamic projections in mammals. Brain Res Bull. 53:727–741.

Sahibzada N, Dean P, Redgrave P. 1986. Movements resembling orientation or avoidance elicited by electrical stimulation of the superior colliculus in rats. J Neurosci. 6:723–733.

Sakata S, Harris KD. 2009. Laminar structure of spontaneous and sensory-evoked population activity in auditory cortex. Neuron. 64:404–418.

Santoro B, Chen S, Luthi A, Pavlidis P, Shumyatsky GP, Tibbs GR, Siegelbaum SA. 2000. Molecular and functional heterogeneity of hyperpolarization-activated pacemaker channels in the mouse CNS. J Neurosci. 20:5264–5275.

Schofield BR. 2009. Projections to the inferior colliculus from layer VI cells of auditory cortex. Neuroscience. 159: 246–258.

Shah MM, Hammond RS, Hoffman DA. 2010. Dendritic ion channel trafficking and plasticity. Trends Neurosci. 33:307–316.

Sheets PL, Suter BA, Kiritani T, Chan CS, Surmeier DJ, Shepherd GM. 2011. Corticospinal-specific HCN expression in mouse motor cortex: I(h)-dependent synaptic integration as a candidate microcircuit mechanism involved in motor control. J Neurophysiol. 106:2216–2231.

Shin M, Brager D, Jaramillo TC, Johnston D, Chetkovich DM. 2008. Mislocalization of h channel subunits underlies h channelopathy in temporal lobe epilepsy. Neurobiol Dis. 32:26–36.

Sholl DA. 1953. Dendritic organization in the neurons of the visual and motor cortices of the cat. J Anat. 87:387–406.

Slater BJ, Willis AM, Llano DA. 2013. Evidence for layer-specific differences in auditory corticocollicular neurons. Neuroscience. 229:144–154.

Sprague JM, Meikle TH Jr. 1965. The role of the superior colliculus in visually guided behavior. Exp Neurol. 11:115–146.

Stafstrom CE, Schwindt PC, Crill WE. 1982. Negative slope conductance due to a persistent subthreshold sodium current in cat neocortical neurons in vitro. Brain Res. 236:221–226.

Stebbings KA, Lesicko AM, Llano DA. 2014. The auditory corticocollicular system: molecular and circuit-level considerations. Hear Res. 314:51–59.

Stein BE. 1978. Nonequivalent visual, auditory, and somatic corticotectal influences in cat. J Neurophysiol. 41:55–64.

Stein BE. 1998. Neural mechanisms for synthesizing sensory information and producing adaptive behaviors. Exp Brain Res. 123:124–135.

Sugimoto S, Sakurada M, Horikawa J, Taniguchi I. 1997. The columnar and layer-specific response properties of neurons in the primary auditory cortex of Mongolian gerbils. Hear Res. 112:175–185.

Sun X, Chen QC, Jen PH. 1996. Corticofugal control of central auditory sensitivity in the big brown bat, Eptesicus fuscus. Neurosci Lett. 212:131–134.

Sun YJ, Kim YJ, Ibrahim LA, Tao HW, Zhang LI. 2013. Synaptic mechanisms underlying functional dichotomy between intrinsic-bursting and regular-spiking neurons in auditory cortical layer 5. J Neurosci. 33:5326–5339.

Suter BA, O'Connor T, Iyer V, Petreanu LT, Hooks BM, Kiritani T, Svoboda K, Shepherd GM. 2010. Ephus: multipurpose data acquisition software for neuroscience experiments. Front Neural Circuits. 4:100.

Takayanagi M, Ojima H. 2006. Microtopography of the dual corticothalamic projections originating from domains along the frequency axis of the cat primary auditory cortex. Neuroscience. 142:769–780.

Thomson AM. 2010. Neocortical layer 6, a review. Front Neuroanat. 4:13.

Ulens C, Tytgat J. 2001. Functional heteromerization of HCN1 and HCN2 pacemaker channels. J Biol Chem. 276: 6069–6072.

Wallace MT, Meredith MA, Stein BE. 1993. Converging influences from visual, auditory, and somatosensory cortices onto output neurons of the superior colliculus. J Neurophysiol. 69: 1797–1809.

Williams SR, Mitchell SJ. 2008. Direct measurement of somatic voltage clamp errors in central neurons. Nat Neurosci. 11: 790–798.

Williams SR, Stuart GJ. 2000. Site independence of EPSP time course is mediated by dendritic I(h) in neocortical pyramidal neurons. J Neurophysiol. 83:3177–3182.

Winer JA. 2006. Decoding the auditory corticofugal systems. Hear Res. 212:1–8.

Winer JA, Larue DT, Diehl JJ, Hefti BJ. 1998. Auditory cortical projections to the cat inferior colliculus. J Comp Neurol. 400: 147–174.

Winer JA, Miller LM, Lee CC, Schreiner CE. 2005. Auditory thalamocortical transformation: structure and function. Trends Neurosci. 28:255–263.

Wu GK, Tao HW, Zhang LI. 2011. From elementary synaptic circuits to information processing in primary auditory cortex. Neurosci Biobehav Rev. 35:2094–2104.

Wurtz RH, Albano JE. 1980. Visual-motor function of the primate superior colliculus. Annu Rev Neurosci. 3:189–226.

Xiong XR, Liang F, Zingg B, Ji XY, Ibrahim LA, Tao HW, Zhang LI. 2015. Auditory cortex controls sound-driven innate defense behaviour through corticofugal projections to inferior colliculus. Nat Commun. 6:7224.

Yan J, Suga N. 1996. Corticofugal modulation of time-domain processing of biosonar information in bats. Science. 273: 1100–1103.

Zhang ZW, Deschenes M. 1997. Intracortical axonal projections of lamina VI cells of the primary somatosensory cortex in the rat: a single-cell labeling study. J Neurosci. 17:6365–6379.

Zhou Y, Liu BH, Wu GK, Kim YJ, Xiao Z, Tao HW, Zhang LI. 2010. Preceding inhibition silences layer 6 neurons in auditory cortex. Neuron. 65:706–717.

Zingg B, Chou XL, Zhang ZG, Mesik L, Liang F, Tao HW, Zhang LI. 2017. AAV-mediated anterograde transsynaptic tagging: mapping corticocollicular input-defined neural pathways for defense behaviors. Neuron. 93:33–47.